

# Deep structure of the Namibia continental margin as derived from integrated geophysical studies

Klaus Bauer,<sup>1</sup> Sönke Neben,<sup>2</sup> Bernd Schreckenberger,<sup>2</sup> Rolf Emmermann,<sup>1</sup> Karl Hinz,<sup>2</sup> Notker Fechner,<sup>3</sup> Karsten Gohl,<sup>3</sup> Albrecht Schulze,<sup>1</sup> Robert B. Trumbull,<sup>1</sup> and Klaus Weber<sup>4</sup>

**Abstract.** During the Geophysical Measurements Across the Continental Margin of Namibia (MAMBA) experiments, offshore and onshore refraction and reflection seismic as well as magnetic data were collected. Together with the existing free-air gravity data, these were used to derive two crustal sections across the ocean-continent transition. The results show that the Early Cretaceous continental breakup and the separation of South Africa and South America were accompanied by excessive igneous activity offshore. Off Namibia we found a 150–200 km wide zone of igneous crust up to 25 km thick. The upper part of this zone consists of an extrusive section comprising three units of basaltic composition: two distinct wedges of seaward dipping reflectors (SDRs) separated by flat-lying volcanic flows. The inner wedge of SDRs can be modeled as the source of a long-wavelength magnetic anomaly that borders long parts of both South Atlantic margins (anomaly G). The crust underneath these extrusives is characterized by high-velocity and high-density material (average values  $7 \text{ km s}^{-1}$ ,  $3 \times 10^3 \text{ kg m}^{-3}$ ). Free-air gravity anomalies along both sides of the high-density crust are interpreted as edge effects resulting from juxtaposition with normal oceanic and continental crust on either side. We define the abrupt landward termination of this zone as the continent-ocean boundary, and consequently, the crust seaward is interpreted as exclusively igneous material and not intruded continental crust. Extrapolation of the interpreted geophysical features along the southwest African margin suggests a fast prograding narrow rift zone and sharp lithospheric rupture leading to the formation of a margin-parallel magmatic belt south of the Walvis Ridge. The influence of the Tristan da Cunha mantle plume may explain the widening of this thick igneous crust near the Walvis Ridge.

## 1. Introduction

Volcanic rifted margins are one of the main categories of large igneous provinces on Earth [Coffin and Eldholm, 1994]. During the last decades the North Atlantic Volcanic Province has emerged as a type example for volcanic margins associated with a prominent mantle plume thanks to the combined interpretations of geophysical data with geological and petrogenetic stud-

ies [Holbrook *et al.*, 1994a; Eldholm and Grue, 1994; Saunders *et al.*, 1997]. The continental flood basalts on the conjugate margins of Namibia and South America and the existence of paired hotspot tracks on the South Atlantic seafloor (Walvis Ridge and Rio Grande Rise) have long been recognized as evidence that the South Atlantic is also flanked by plume-related volcanic margins [O'Connor and Duncan, 1990]. Marine reflection seismic data support this interpretation with the recognition of seaward dipping reflector (SDR) sequences on both sides of the South Atlantic [Light *et al.*, 1993; Gladchenko *et al.*, 1997; Hinz *et al.*, 1999]. Figure 1 shows the distribution of seaward dipping reflector sequences offshore and flood basalts onshore in the South Atlantic region. It is important to note that both the continental flood basalts and the seaward dipping reflectors appear limited to the margins south of the hotspot traces.

Previous studies have addressed many different aspects of the rifting and continental breakup at the Namibian margin. These include studies of the geol-

<sup>1</sup>GeoForschungsZentrum Potsdam, Potsdam, Germany.

<sup>2</sup>Bundesanstalt für Geowissenschaften und Rohstoffe, Hannover, Germany.

<sup>3</sup>Alfred-Wegener-Institut für Polar- und Meeresforschung, Bremerhaven, Germany.

<sup>4</sup>Institut für Geologie und Dynamik der Lithosphäre, Universität Göttingen, Göttingen, Germany.

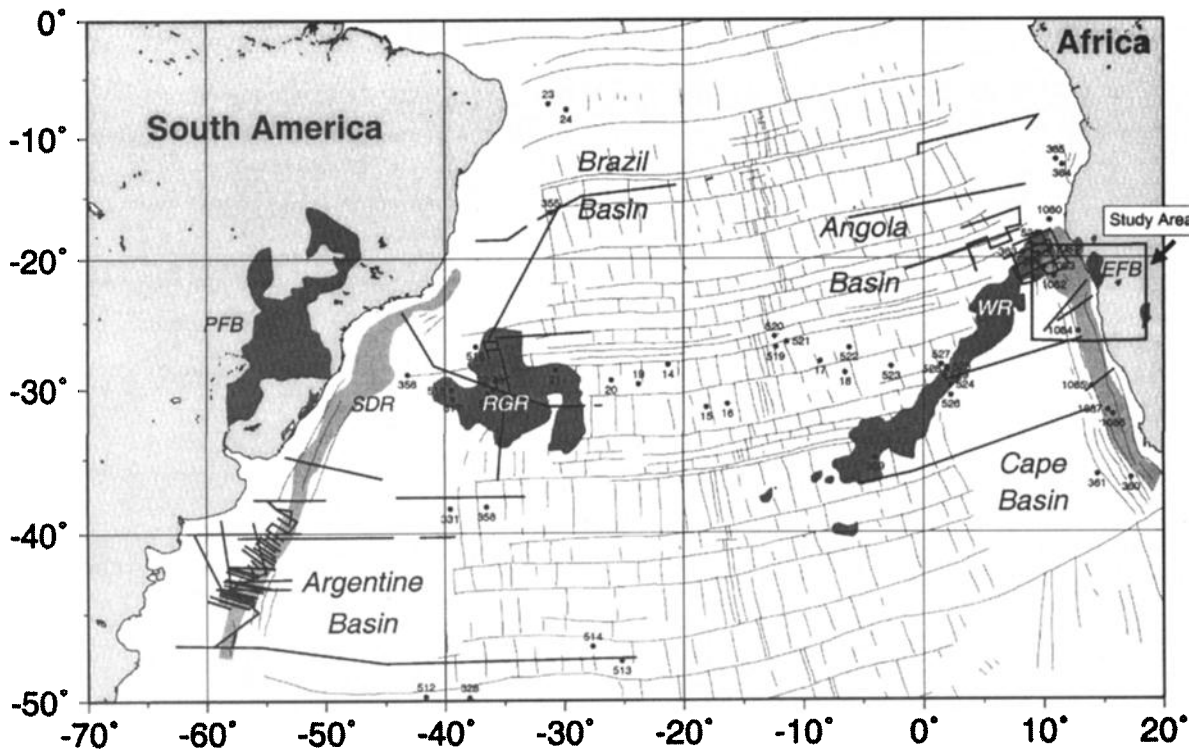


**Figure 1.** Magmatic features related to the Mesozoic opening of the South Atlantic ocean, indicated by PFB, Paraná flood basalts; RGR, Rio Grande Rise; WR, Walvis Ridge; EFB, Etendeka flood basalts. Distribution of seaward dipping reflectors (SDRs) are shown that have been recognized during previous surveys. Locations of BGR reflection seismic profiles (including this study) and DSDP/ODP drill sites are indicated by numbered dots.

ogy and petrogenesis of igneous complexes [e.g., Martin *et al.*, 1960; Erlank *et al.*, 1984; Milner and LeReox, 1996; Trumbull *et al.*, 1997; Ewart *et al.*, 1998]; interpretation of offshore reflection seismic profiles [Austin and Uchupi, 1982; Light *et al.*, 1993; Gladczenko *et al.*, 1997], studies of magnetic seafloor anomalies [Rabinowitz and LaBrecque, 1979; Nürnberg and Müller, 1991], gravity models [Rabinowitz and LaBrecque, 1979; Light *et al.*, 1992], and models for uplift and erosion derived from apatite fission track data [Brown *et al.*, 1990; Gallagher and Brown, 1997].

However, the deep-crustal seismic data and velocity-depth models needed for a complete interpretation of the Namibian margin had previously been lacking, and the investigations reported here were designed to provide that information. A combined onshore-offshore multichannel and wide-angle seismic survey was carried out in December 1995 by the Bundesanstalt für Geowissenschaften und Rohstoffe, Hannover (BGR), the Alfred-Wegener-Institut für Polar- und Meeresforschung, Bremerhaven (AWI), and the GeoForschungsZentrum, Potsdam (GFZ). The offshore portion of the experiments was designed to obtain complete two-dimensional (2-D) crustal sections across the continent-ocean boundary; to confirm the existence of high-velocity bodies in the lower crust below the SDRs,

postulated by Gladczenko *et al.* [1997]; and to assess the cause of the prominent magnetic anomaly G [Rabinowitz and LaBrecque, 1979]. Onshore, the goals of the experiments were to map the variations in Moho depth from the continent-ocean boundary onto stable continental crust and to reveal the deep structure of the continental crust in a region that was intruded by breakup-related igneous complexes. This paper presents the results and interpretations of two profiles that traverse the continental margin in the late Precambrian Damara Belt (Figure 2).

## 2. Geological and Geophysical Setting

The seismic transects 1 and 2 traverse deeply eroded basement rocks of the late Precambrian Damara Orogen. Transect 1 crosses a region of the Damara basement, which has been strongly affected by Cretaceous breakup-related igneous activity. The transect lies just south of the Etendeka flood basalts, the largest exposures of continental flood basalts in Namibia, and it directly crosses two Cretaceous intrusive complexes (Cape Cross and Messum, see Figure 2). Transect 2 intersects the coastline ~150 km farther south, in an area of the Damara basement that is less affected by Cretaceous activity and is more deeply eroded.

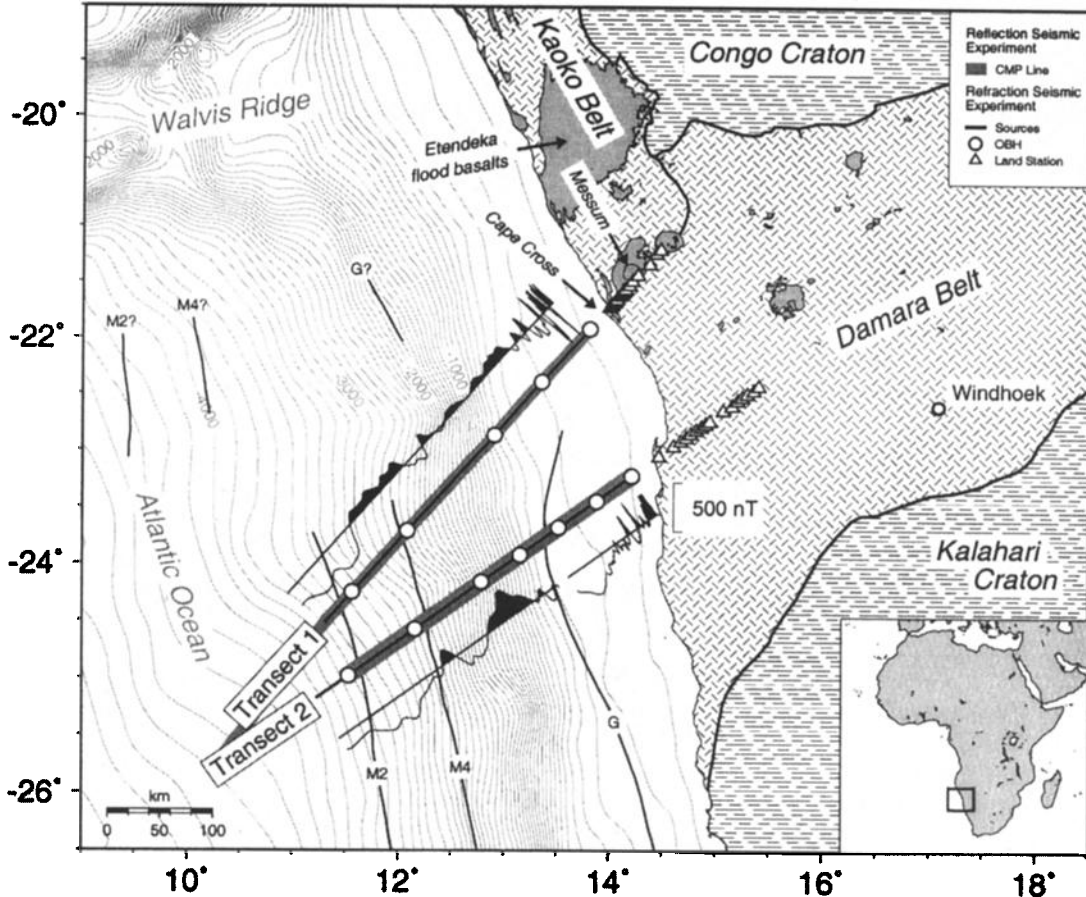


**Figure 2.** Location map, showing the geometry of the reflection and refraction seismic experiment and wiggle traces of the simultaneously measured magnetic data. Magnetic lineaments after Rabinowitz and LaBrecque [1979] are given as well as simplified geology of the Damara orogeny and Mesozoic igneous complexes (shaded).

### 2.1. Prerift Geology: The Damara Orogen

The Damara Orogen is part of the late Precambrian Pan-African fold system, which affected much of the western margin of Africa and has its equivalents on the Atlantic coast of South America [Porada, 1979, 1989]. The orogen consists of a coastal arm (Kaoko Belt in the north and Gariep Belt in the south) along which a proto-Atlantic Ocean opened [Porada, 1979], and an inland arm, the Damara Belt proper, which strikes NE-SW. Reviews of the geology of the Damara Orogen are given, e.g., by Miller [1983] and Tankard *et al.* [1982].

The Damara Belt itself is a deeply eroded fold belt some 400 km wide, which separates the Congo Craton and Kalahari Craton (Figure 2). It is subdivided into a number of tectonostratigraphic zones, which in part outline the position of late Proterozoic NE-SW trending rift structures filled with thick metasedimentary sequences. Subsequent convergence of the bounding cratons caused intense NW-SE directed compressional and transpressional deformation with inversion of the rift structures, medium to high-grade regional metamorphism, and granite emplacement.

### 2.2. Mesozoic Volcanism, Rifting, and Continental Breakup

After erosion of the Damara Orogen, sedimentation began in the late Paleozoic with glacial deposits of the Dwyka Group, and this was followed in the Permian and Triassic by continental and shallow marine sedimentation, which formed the upper units of the Karoo Supergroup. Sedimentation terminated with outflow of the olivine-normative flood basalts of the Drakensberg Group, whose age is 186–183 Ma [Duncan *et al.*, 1997]. Karoo age volcanics are of much less importance in central Namibia than in South Africa, and the main focus of Mesozoic magmatism was in the early Cretaceous at the site of the present Atlantic coast, where continental flood basalts (Paraná-Etendeka Province) were emplaced on both sides of the present Atlantic Ocean. The continental flood basalts now cover an area of some 800,000 km<sup>2</sup> and the volume of erupted magma is estimated at a minimum of  $\sim 2 \times 10^6$  km<sup>3</sup> [Peate, 1997]. Controversy continues about the process of mantle melting producing this huge volume of basalts and about whether, or in what manner, a man-

tle plume was involved [Arndt and Christensen, 1992; Turner et al., 1996; Peate, 1997].

A further important expression of the Cretaceous magmatism in Namibia is the emplacement of a large number of subvolcanic ring-type intrusive complexes (the Damaraland complexes) and mafic dike swarms. The Damaraland complexes as a group comprise of a great variety of rocks including carbonatites, syenites, gabbros, and granites [Martin et al., 1960]. Two of these complexes are crossed by the onshore part of seismic transect 1: Cape Cross at the present coastline and Messum, some 50 km farther inland (Figure 2). The Cape Cross intrusion is only poorly exposed at the coastline, but aeromagnetic data show that more than half of it is located offshore [Eberle et al., 1996]. The exposed rocks at Cape Cross are granites, gabbros, and syenites. Messum consists of concentric ring dikes of gabbros, anorthosite, granitoids, and syenites, with a central intrusion of syenites, microgranites, and rhyolite [Korn and Martin, 1954; Harris et al., 1999]. The gabbros and syenites from Messum and the basalts associated with the complex have O, Sr, and Nd isotopic compositions, which indicate a mantle origin [Harris, 1995; Trumbull et al., 1997; Ewart et al., 1998; Harris et al., 1999].

Radiometric dating has shown that eruption of the continental flood basalts and emplacement of several of the intrusive complexes took place over a very narrow interval of time at  $132 \pm 1$  Ma [Milner et al., 1995; Renne et al., 1996, 1997; Schmitt et al., 2000]. The oldest magnetic seafloor-spreading anomaly recognized off Namibia is correlated with M4 (circa 130 Ma [Rabinowitz and LaBrecque, 1979]), which therefore indicates that the continental magmatism took place only shortly before or simultaneously with the onset of seafloor spreading. Apatite fission track data of Brown et al. [1990] indicate a phase of rapid denudation at 125 Ma in the coastal area of central Namibia, where an estimated 3000 m have been removed by erosion, particularly in the early Cretaceous. In the area of the central Damara Belt and the seismic traverses, apatite fission track data of Haack [1983] show that young ages (<130 Ma) extend much farther inland than in the south, a fact that may reflect a greater degree of Mesozoic cover in this area and/or the thermal effect of the Damaraland intrusive complexes. Estimates of the thickness of volcanic cover once present above the intrusive complexes suggest that in this area, too, some 3000 m of section was removed by uplift and erosion.

### 2.3. Previous Geophysical Surveys

Some 14,000 km of commercial reflection seismic profiling, with concurrent gravity and magnetometry surveys, were carried out on the Namibian continental shelf to aid in hydrocarbon exploration [Light et al., 1992, 1993]. Most of the seismic profiles were recorded to a maximum of 7 s two-way time, and information about the deep crustal structure is therefore limited.

On the basis of these data, Light et al. [1992] distinguished four stages of basin development on the margin: prerift, synrift I, synrift II, and drift/thermal sag phase. Drilling results confirm that the rift basins contain interbedded aeolian sands and basalts of the Etendeka formation. Light et al. [1992] also comment on the presence of a coast-parallel free-air gravity high. Lacking deep-crustal seismic data, they were only able to speculate that the anomaly was due to Moho topography under a crust thinned by simple shear extension. The possibility of dense magma underplating the crust was not discounted.

Gladzenko et al. [1997, 1998] emphasized features of the Namibian margin related to magmatism using commercial multichannel seismic (MCS) data and gravity data from Namibia and also discussed parallels with the conjugate margin of Argentina. They interpreted the transition between normal oceanic and continental crust as a ~150-km-wide rift zone partly covered by dipping wedges which borders on thick oceanic crust with seaward dipping reflectors.

Three land-based explosion-seismic refraction profiles were carried out in 1975 in the central zone of the Damara Orogen [Baier et al., 1983; Green, 1983]. The results show an upper crust of dominantly felsic material ( $v_p = 5.9\text{--}6.2$  km/s), which extends to ~15 km depth. Below that depth the seismic velocity jumps to 6.4 km/s. According to Green [1983], material with that velocity extends down to the Moho at 40–50 km depth, whereas Baier et al. [1983] suggested that higher-velocity material ( $v_p = 7\text{--}8$  km/s) may be present in the lower crust at 30–50 km depth and interpreted this to indicate magmatic underplating. Our seismic transect 2 aligns with profile 1 of Green [1983], which failed to detect a Moho reflection because it traverses very thick sedimentary sequences. Green [1983] inferred a crustal thickness of ~55 km for this area on the basis of gravity data.

## 3. Acquisition, Processing and Modeling

The experiments reported here included the acquisition of seismic reflection and refraction/wide-angle reflection data as well as magnetic surveys. In addition, we have compiled the available satellite-derived free-air gravity data for the region [Sandwell and Smith, 1997]. This section discusses the acquisition, processing, and integrated modeling of these data sets.

### 3.1. Seismics

**3.1.1. Data acquisition and processing.** The seismic data were acquired during a two-ship marine survey involving the Russian vessel R/V *Akademik Nemčinov* and the Norwegian vessel R/V *Polar Queen*. The seismic refraction/wide-angle reflection investigations involved synchronous data collection by ocean bottom hydrophones (OBH) operated by AWI and onshore seismometers of the GFZ (see Figure 2). Source signals

were generated by a tuned air gun array of 54 L (partly augmented by two 33 L air guns) fired at 60-s intervals, which corresponds to 140-m source spacing. The distance between the OBHs varied between 40 and 70 km. On land, 25 recorders equipped with three-component 1-Hz seismometers were deployed, with spacing of 2.5 km (in the coastal region) to 15 km (on the northeastern end of the lines). Sampling interval was 10 ms.

A total of 2806 km of MCS data were acquired by BGR using R/V *Akademik Nemčinov*. The data were collected along the refraction/wide-angle reflection lines and an additional 1737 km of pure MCS profiles were measured from the continental shelf to the deep Cape Basin off Namibia. The reflection seismic equipment consisted of a Sercel SN 358 DMX digital recording system, a 3000-m, 240-trace streamer, and four air gun arrays with 32 guns having a total volume of 53.4 L. The operating pressure was 135 bars; shot intervals on pure MCS profiles were 150 m and 50 m, with nominal coverage of 10-fold and 30-fold, respectively.

The refraction data were compiled as receiver gathers for each OBH and land station. The raw land data are of excellent quality, whereas some of the OBH data were partly affected by instrumental noise. The latter was suppressed using predictive deconvolution. Further data-processing steps included band-pass filtering and frequency-wavenumber (FK) filtering in cases of strong noise from previous shots. Dominant frequencies are  $\sim 8$  Hz. The data also show clear *S* wave signals resulting from conversions at the ocean bottom and crustal boundaries, which, however, are not considered in this paper.

The reflection MCS data were processed on ship to the stage of a stacked version. Conventional processing routines consisting of geometry application and common mid point (CDP) sorting were applied. Velocity analyses were done every 3.5 km. After minimum phase predictive deconvolution, multiples attenuation, and dynamic corrections the traces of the CDP gathers were stacked. These stacked CDP traces were band-pass filtered and normalized. The stacked data were time migrated using an FK algorithm.

**3.1.2. *P* velocity modeling and imaging: Procedures and reliability.** The seismic velocity models of the crust were derived using both the refraction/wide-angle reflection data and MCS data. The former yield *P* velocities and roughly locate major discontinuities down to upper mantle levels, whereas the MCS data provide reflectivity patterns of the crust and highly resolved discontinuities, albeit often limited to shallower crustal depths. Thus the combination of both types of data increases the reliability of the *P* velocity models by providing geometric constraints and allows for better founded conclusions on the physical and chemical properties of the crust. We used the following procedures to establish 2-D time sections and depth sections, each comprising *P* velocities and reflection seismic results.

In the first step the models were developed in the offshore regions for the upper section above the acoustic basement. For each OBH, travel times of primary *P* wave phases at small distances ( $<30$  km) were determined, and forward modeling was applied with 2-D ray tracing methods [Zelt and Smith, 1992]. Several layers were established on the basis of diving phases and some reflection arrivals. We assumed linear lateral *P* velocity variations between the well-resolved OBH locations. Vertical *P* velocity gradients were estimated from travel time curvatures. The topography of unresolved parts of the layer boundaries was constrained by the corresponding near-vertical reflections identified in the MSC data.

Once the sequence from seafloor to acoustic basement was fixed in the models, crustal and uppermost mantle *P* velocities were determined on the basis of both the OBH and land station wide-angle data. Unfortunately, the MCS data could not be used for additional constraints because of its poor imaging of the subbasement structures. Again, we forward modeled travel times using the 2-D ray tracing module of Zelt and Smith [1992]. This method has limitations in strongly heterogeneous media, and in such cases, where rays could not be traced through complicated regions of the model, first arrival times were calculated by the use of wave front tracing [Podvin and Lecomte, 1991]. The velocity distribution of the upper and middle crust was determined using diving-wave arrivals. The high-quality land data permitted identification of crustal diving phases from greater depths as secondary arrivals, which gave some control on the lower crustal velocities. Otherwise, the *P* velocities of the lower crust had to be determined from travel times of wide-angle reflections. The velocity of a layer just above the Moho was estimated from amplitude modeling [Zelt and Ellis, 1988] of wide-angle reflections from the top and bottom of this body. The depth of the Moho was constrained by wide-angle reflection arrivals and a few arrivals of upper mantle diving waves. The latter also gave some control on *P* velocities of the uppermost mantle. In some cases, we used the facility of the ray tracing module of Zelt and Smith [1992] to model floating reflectors in the middle crust, which could not be resolved as velocity discontinuities.

The reliability of the final *P* velocity models depends on a number of factors including the accuracy of the individual travel time picks (0.03–0.1 s), the uncertainty of measured apparent velocities of the corresponding phases, the type of phases used, and the ray coverage. In our case, the dense spatial sampling allows for good phase correlation and reliable determination of apparent velocities. Further constraints were given by the MCS reflection data and amplitude modeling. We estimated uncertainties of velocities and depths of boundaries by perturbation of selected velocity and depth parameters [Zelt, 1999]. For the section above the acoustic basement and the uppermost crust the error in *P* wave velocities is about  $\pm 0.1$  km/s and about  $\pm 0.3$  km in

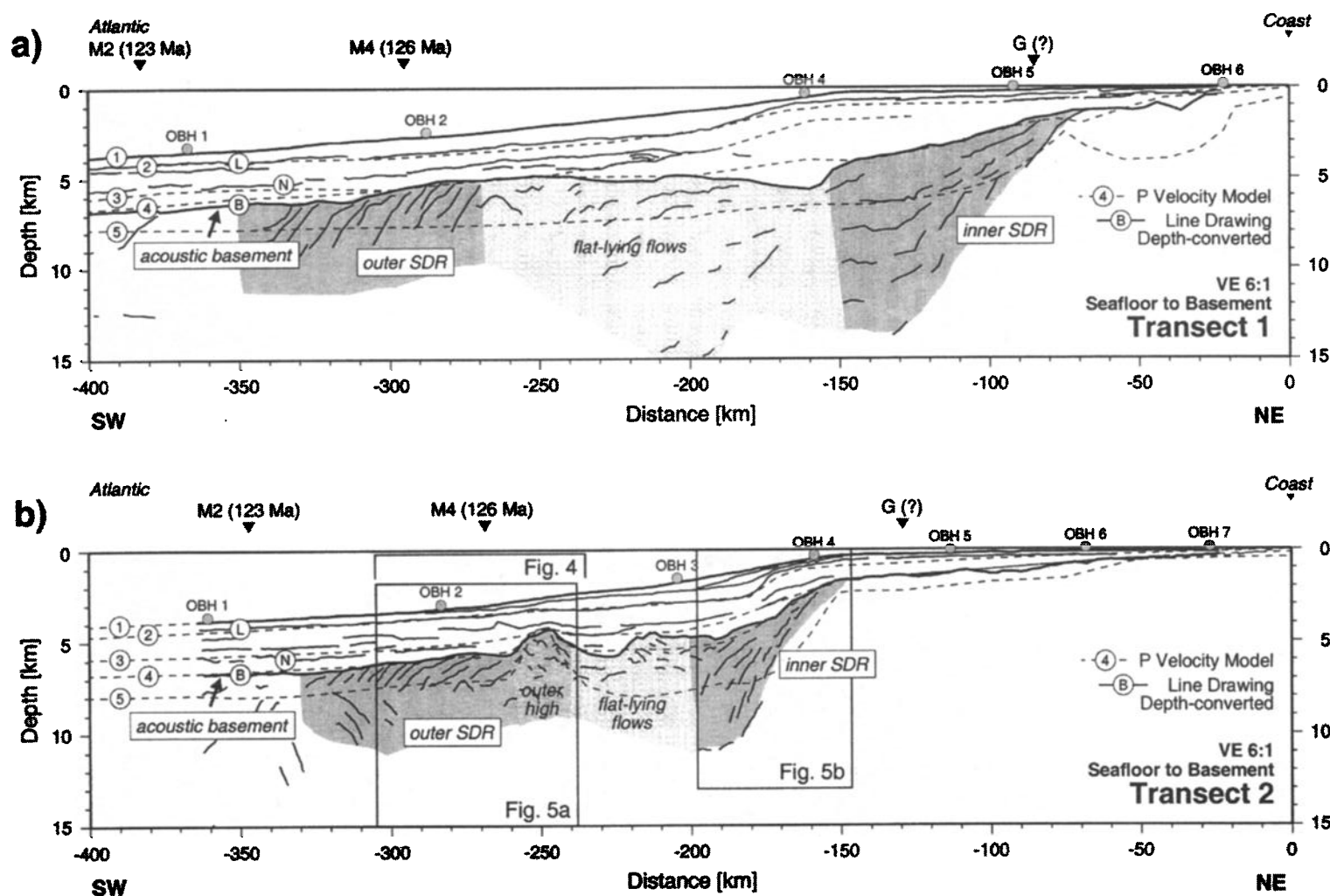


**Figure 3.** Interpretation of reflection seismic data which were measured along transects (a) 1 and (b) 2. Line drawings from time-migrated data were depth converted using the final  $P$  velocity models. Defined regions of distinct reflectivity patterns (e.g., SDR, seaward dipping reflections) are indicated. Superimposed are layer boundaries of the corresponding uppermost parts of the  $P$  velocity models.

depth determination. The error in the velocity of the deeper crust (>15 km) is about  $\pm 0.2$  km/s, and the depth determination of boundaries is accurate to about  $\pm 3$  km. Uncertainties in  $P$  velocities in the uppermost mantle are about  $\pm 0.15$  km/s.

Regions of the models that are only covered by rays to the onshore stations are inherently nonunique because of the limited distance window of the registrations. This problem in our study is partly compensated for by the dense receiver spacing and the fact that parts of the ray paths are well defined by reversed OBH registrations and MCS data. Further important constraints came from geological and geophysical knowledge [Milner, 1997; Baier et al., 1983; Green, 1983], from which we could exclude a sedimentary succession with low velocities beneath the onshore receiver sites. For the re-

gions of the models that are affected by this problem, which are indicated in the following figures, estimated uncertainties in the velocities are about  $\pm 0.1$ - $0.15$  km/s in the upper and middle crust (<20 km) and  $\pm 0.2$  km/s in the lower crust and uppermost mantle. Uncertainties in the depth determination of the Moho are  $\sim 3$ - $5$  km.

The  $P$  velocity models were finally used to depth convert line drawings of the time-migrated reflection seismic data. A fine grid of rectangular cells (0.1 by 0.01 km, width by height) with constant  $P$  velocity was calculated from the velocity models and for each distance-time pair, a depth was determined from the sum of two-way times of grid cells at the corresponding location.

**3.1.3. Seafloor to basement sequence.** Figure 3 shows 2-D depth sections along transects 1 and 2 down to acoustic basement levels. The sections combine the

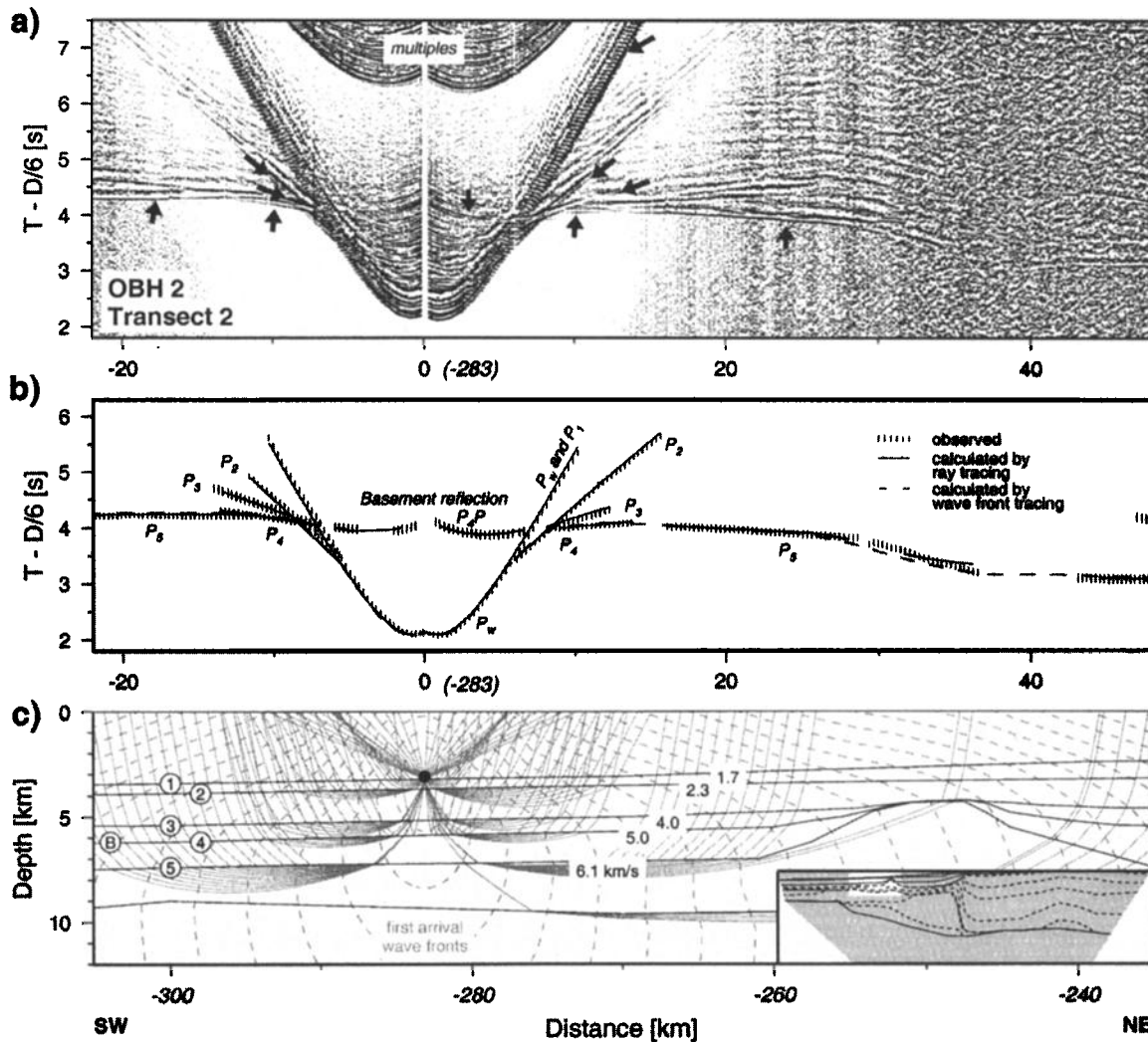


**Figure 4.** (a) Receiver gather comprising small-offset recordings of OBH 2 on transect 2. The vertical axis corresponds to reduced travel time (reduction velocity is 6 km/s). Distances represent shot-receiver offsets (regular type) and model coordinates of transect 2 (italic type), respectively. Amplitudes have been trace normalized. (b) Observed and calculated travel times based on the final  $P$  velocity model for transect 2. (c) Corresponding model section showing ray paths and first arrival wave fronts.

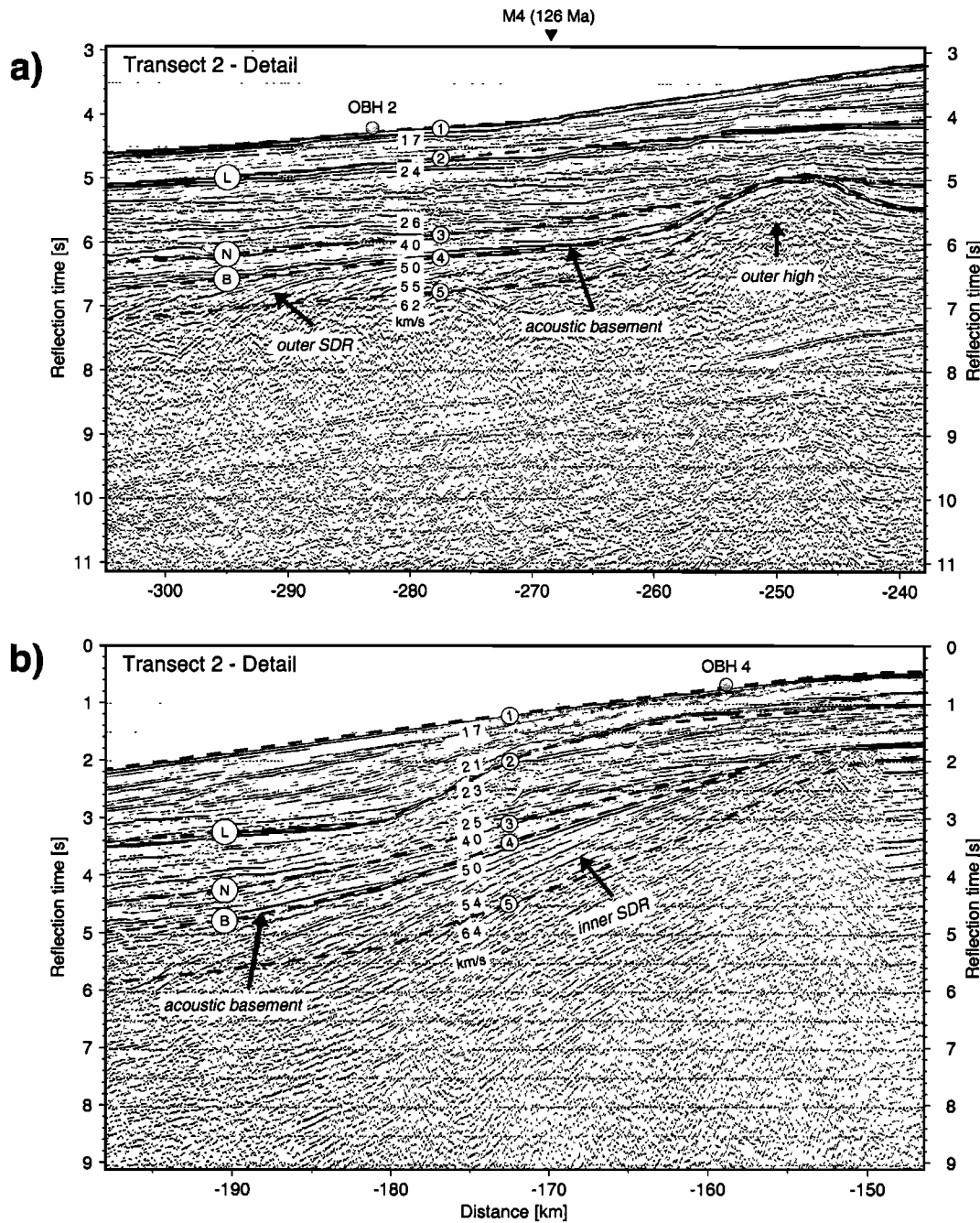


**Figure 5.** Seismogram examples (time migrated) from transect 2 (see Figure 3) showing (a) the outer and (b) the inner wedge of SDRs with superimposed  $P$  velocity model. Layer boundaries of the latter were depth to time converted.

interpretation of the reflection seismic data and the uppermost boundaries of the final  $P$  velocity models (1–5, with 1 representing the seafloor). Coherent signals in the reflection data were marked by line drawings. The prominent horizons marked L and N were identified by comparison with former studies in this region [Gerrard and Smith, 1982; Light et al., 1992]. These boundaries correspond approximately to interfaces 2 and 3 of the  $P$  velocity models, respectively. The top of the acoustic basement B was defined by the most promi-

nent and extensive reflection and coincides with boundary 4 of the  $P$  velocity models. Beneath this horizon, regions of distinct reflectivity patterns were identified (e.g., seaward dipping reflections, flat-lying and mound-like structures), and these are outlined in different patterns of shading on Figure 3.

Examples of data and modeling are given in Figures 4 and 5 for subregions of transect 2 (see outlines in Figure 3b). The identification and fitting of phases in the OBH data are shown for OBH 2 in Figure 4.  $P_1$  to  $P_4$  repre-

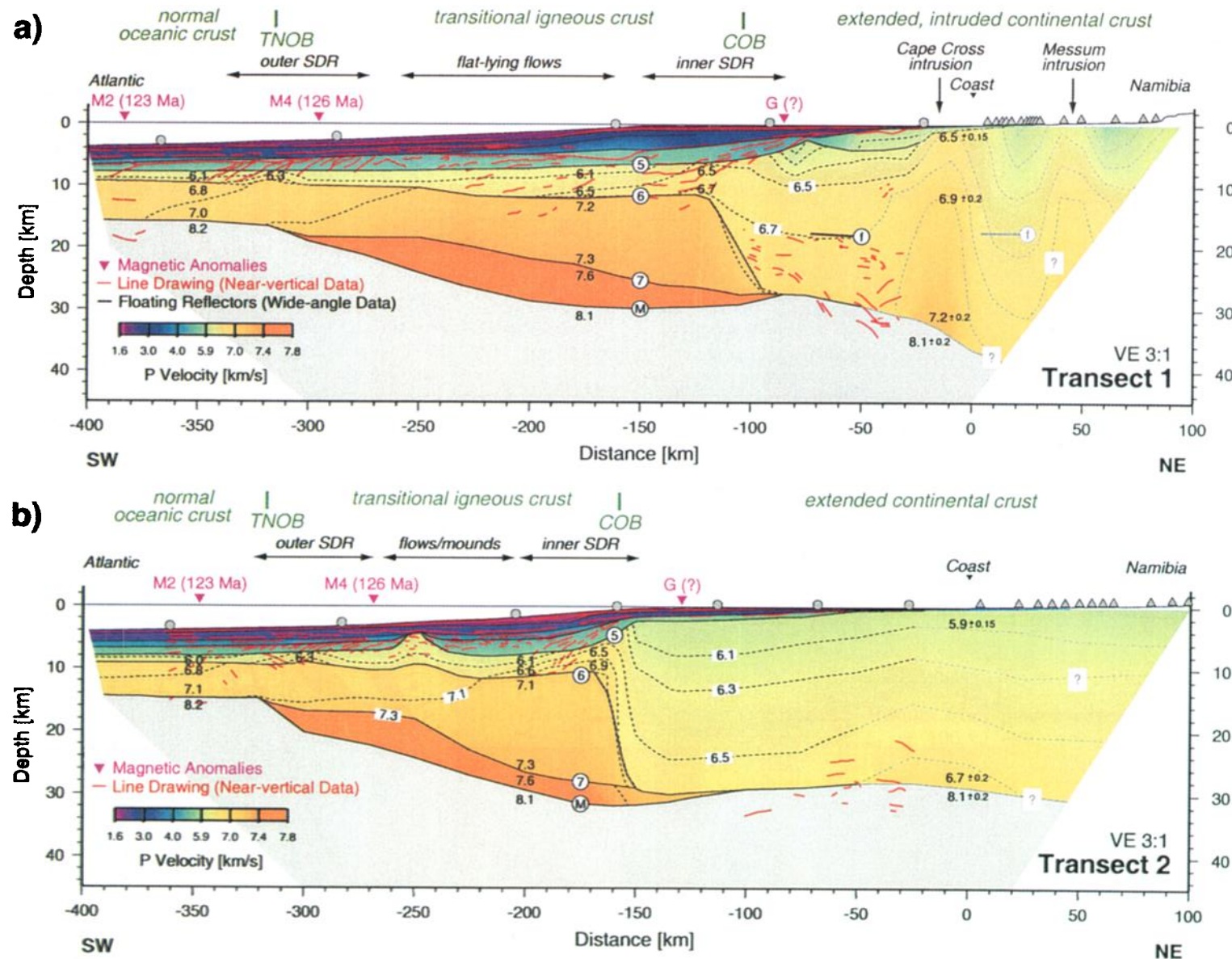


**Plate 1.** Interpreted crustal depth sections along transects (a) 1 and (b) 2, combining  $P$  velocities, floating reflectors, and depth converted line drawings. Solid black lines represent  $P$  velocity discontinuities of first order, while dashed lines are isovelocity lines. The isovelocity lines are drawn fainter in regions where uncertainty is high due to the lack of small-offset and reversed observations onshore. COB, continent-ocean boundary; TNOB, transitional-normal oceanic crustal boundary.

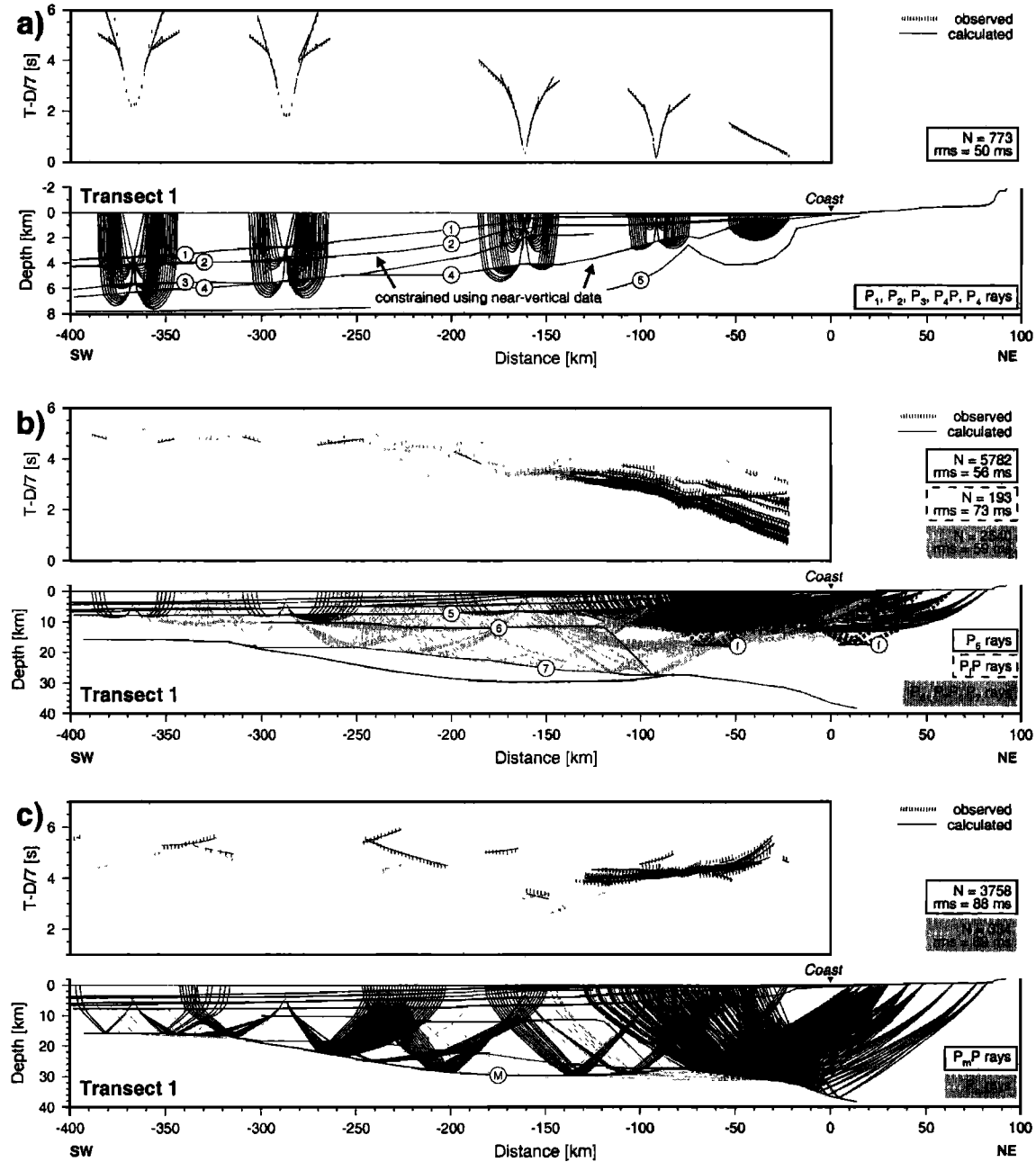


**Figure 6.** Observed and calculated travel times (N, number of picks; rms, total root-mean-square error) and corresponding ray paths for transect 1. Separate depth levels: (a) upper layers down to the acoustic basement using phases  $P_1$ ,  $P_2$ ,  $P_3$ ,  $P_4P$ , and  $P_4$ , (b) upper and middle crust ( $P_5$ ), midcrustal floating reflectors ( $P_fP$ ) and the middle and lower crustal regions ( $P_6$ ,  $P_7P$ , and  $P_7$ ), and (c) the Moho ( $P_mP$ ) and the uppermost mantle ( $P_n$ ).

sent refracted phases diving beneath the interfaces 1-4. The  $P_4P$  reflection from interface 4 corresponds with the top of the acoustic basement as defined with the near-vertical data. The layer coinciding with the seaward dipping reflectors beneath the basement reflector is characterized by velocities of 5–5.5 km/s. Beneath this, velocities >6 km/s are required to explain the  $P_5$  first arrivals at offsets larger than 15 km. Note the early  $P_5$  arrivals at offsets between 30 and 40 km (-255 and -245 km in model coordinates). In order to fit this travel

time anomaly, an updoming of boundaries 4 and 5 was incorporated in the model.

Figure 5 shows the relationship between the derived  $P$  velocity model and the reflection seismic images and demonstrates the interpretation of the latter in terms of reflection horizons and reflectivity patterns. The  $P$  velocities vary only slightly within the layers and are consistent with the model developed for transect 1. The sequence in Figure 5a is similar to the modeling example discussed above (Figure 4), and it shows that the

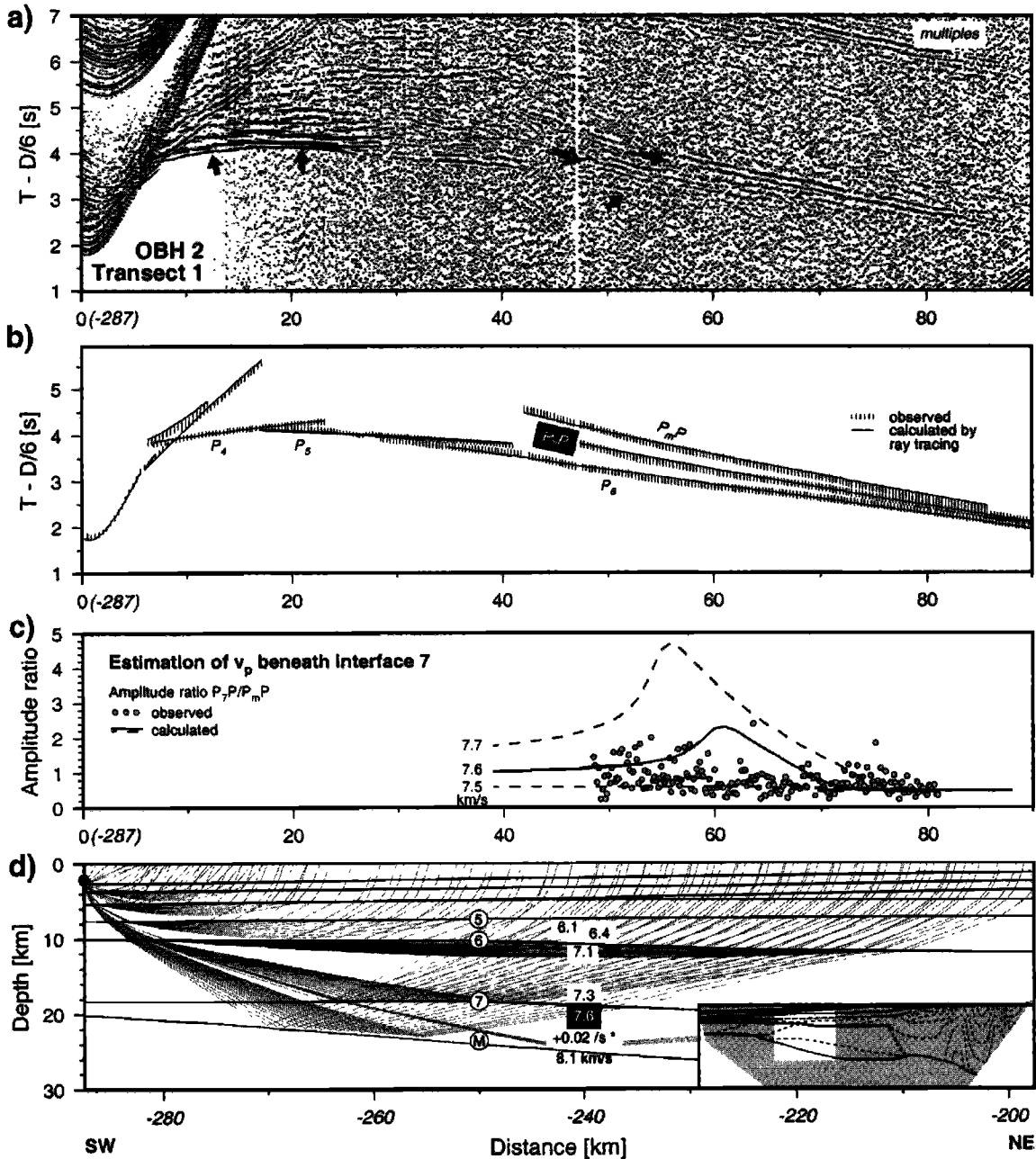
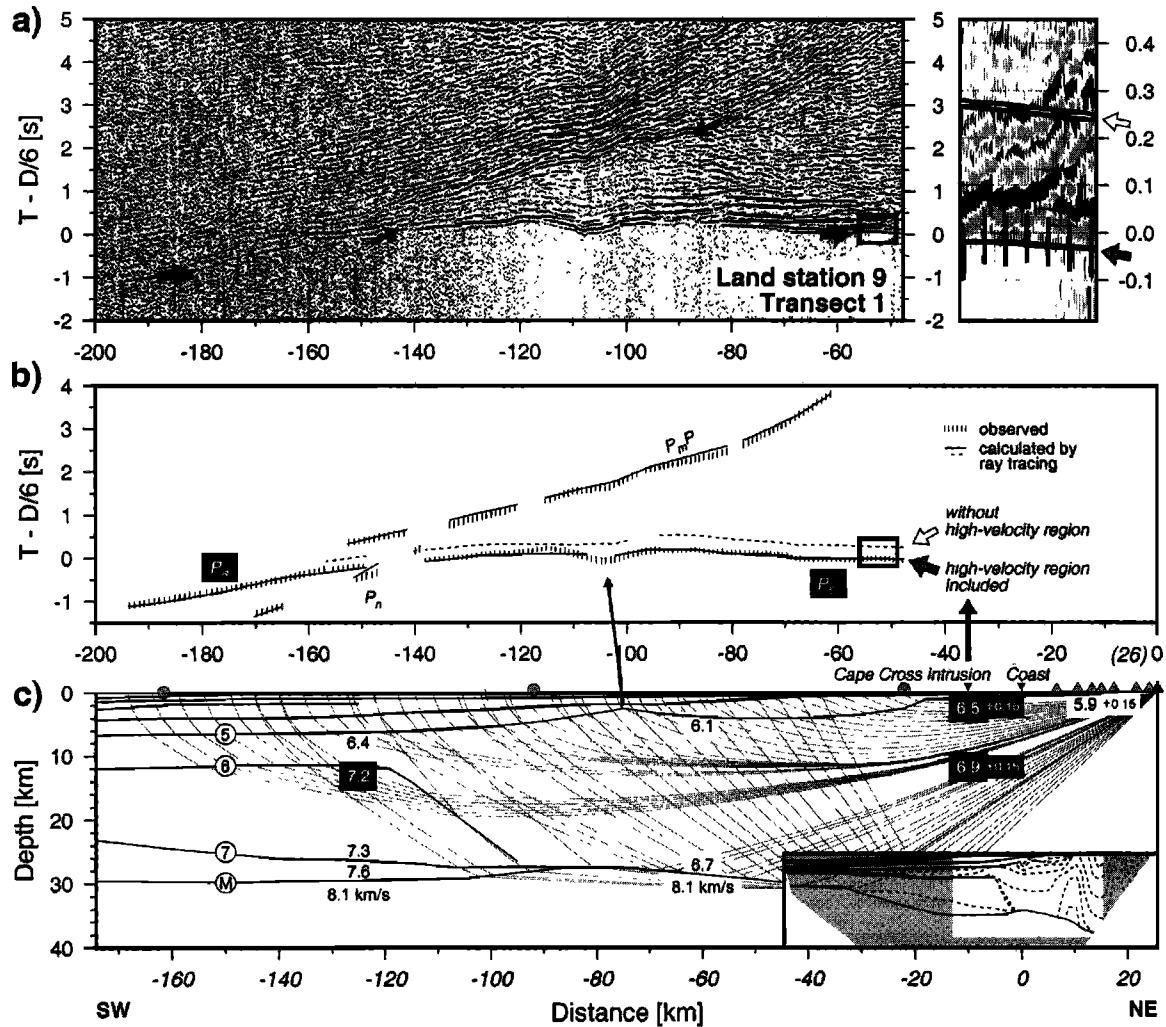


**Figure 7.** Record section for OBH 2 on transect 1. (a) Data displayed as in Figure 4. (b) Observed and calculated travel times based on the final  $P$  velocity model for transect 1 (Plate 1a). (c) Estimation of the velocity beneath interface 7 from modeling the amplitude ratio of wide-angle reflections  $P_7P$  and  $P_mP$ . (d) Corresponding model section showing ray paths.

velocity discontinuities constrained by wide-angle observations are in good agreement with the marker horizons L, N, and B. Furthermore, the superposed velocity model reveals that each velocity layer corresponds to a sequence of distinct reflectivity in terms of strength, frequency, and coherency. The entire succession above the basement is dominated by subparallel and partly prograding patterns. Neither horizon N or L nor the top of the acoustic basement B is apparently offset by faulting. Both SDR regions comprise stacks of bent continuous reflections, which diverge seaward and con-

verge landward at the basement reflector. The base of these zones coincides roughly with the transition to the layer beneath interface 5, but it is not well defined in the reflection images.

**3.1.4. Crustal architecture.** Plate 1 shows the final  $P$  velocity distribution and depth-converted line drawings derived for the entire crust along transects 1 and 2. Both crustal sections extend to 400 km offshore, including the rise, slope, and shelf, and 100 km on land. In addition to the five boundaries which were shown in Figure 3 and discussed in section 3.1.3, the sections in



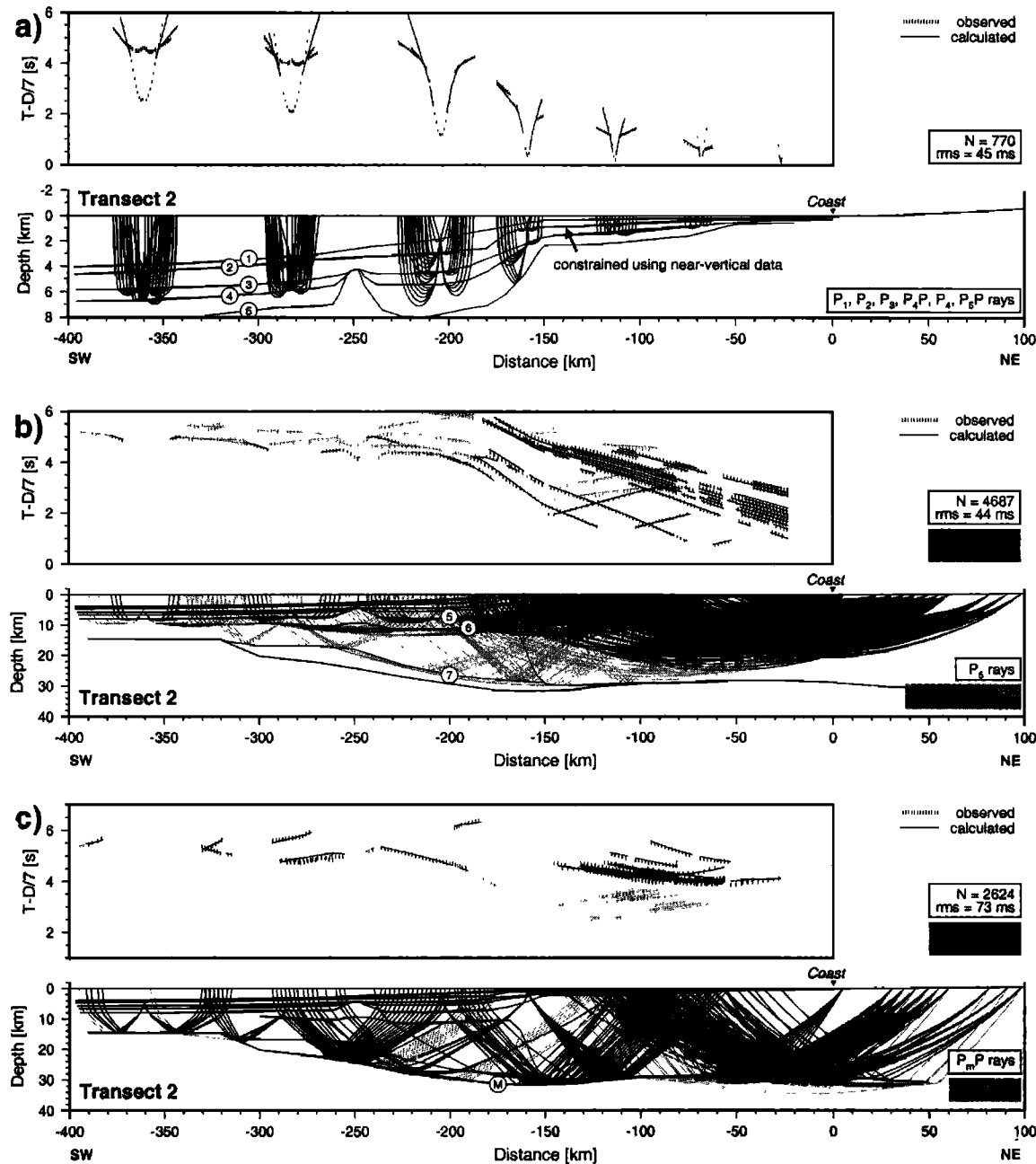
**Figure 8.** Seismic data recorded by the vertical component of land station 9 on transect 1. (a) Data displayed as in Figure 4. The detail illustrates the wave field and travel time fitting of phase  $P_5$  (Figures 8b and 8c). (b) Observed and calculated travel times based on the final  $P$  velocity model for transect 1 (Plate 1a). (c) Corresponding model section showing ray paths.

Plate 1 show first-order discontinuities 6 and 7 and the crust-mantle boundary M. Both transects are characterized by strong lateral variations of the crustal velocities as indicated in Plate 1 by dashed isolines. The most prominent feature of both transects is a high-velocity zone ( $>7$  km/s) in the middle and lower crust between -300 and -100 km on transect 1 and -300 to -150 km on transect 2. This zone underlies the regions with distinct reflectivity patterns, including SDRs mentioned above. At the base of the high-velocity zone is a layer with velocities of  $\sim 7.6$  km/s.

Crustal velocities decrease abruptly landward of this high-velocity zone in the entire crustal section. We identify this strong lateral velocity gradient as the continent-ocean boundary (COB; see discussion below). On transect 1, steeply bounded regions of enhanced velocity were modeled at about -15 km and 35 km. The near-vertical data (line drawings) and wide-angle

data (floating reflectors) reveal lower crustal reflectivity around these high-velocity regions. The lower crustal reflectivity appears to disappear oceanward of the COB, which could be due to a masking effect of the overlying material or could indicate a real change in the elastic properties of the lower crust. We define a further crustal boundary near the NW end of the transects, which is defined by a change in depth and topography of the Moho and is indicated in Plate 1 as transitional-normal oceanic crustal boundary (TNOB). The Moho varies considerably in depth along the transects, from  $\sim 15$  km in the southwest to 35-40 km onshore. In some parts of the transect a reflection Moho (line drawing) could be identified, and where present, its location is in agreement with the velocity models.

To support the derived crustal sections, Figures 6-11 present overviews and examples of data and modeling for each transect including OBH and land data. Fig-



**Figure 9.** Observed and calculated travel times ( $N$ , number of picks;  $\text{rms}$ , total root-mean-square error) and corresponding ray paths for transect 2. Divided into separate depth levels: (a) upper layers down to the acoustic basement using phases  $P_1, P_2, P_3, P_4P, P_4$ , and  $P_5P$ , (b) upper and middle crust ( $P_5$ ) and the middle and lower crustal regions ( $P_6, P_7P$ , and  $P_7$ ), (c) the Moho ( $P_mP$ ) and the uppermost mantle ( $P_n$ ).

ure 6 shows the ray coverage and travel time fitting for transect 1. The data from OBH 2 on transect 1 (Figure 7) show clear first arrivals, which were used to adjust the crustal velocities. The intracrustal boundary 7 is based on the wide-angle reflection phase  $P_7P$  observed at offsets between 30 and 70 km. The Moho reflection can be identified at offsets  $>40$  km. Because we have no direct velocity information from refracted arrivals for the layer beneath interface 7, we estimated its value

by modeling the amplitude ratio of the  $P_7P$  to  $P_mP$  wide-angle reflections (Figure 7c). For this purpose, the entire model was fixed except for velocity just beneath boundary 7, while the vertical velocity gradient of 0.02 /s in this layer was extrapolated from the layer above it. Velocities of  $7.6 \pm 0.1$  km/s produce reasonable relative amplitude variations with offset.

Figure 8 shows an example of an onshore receiver gather from transect 1. To explain the  $P_5$  arrivals ob-

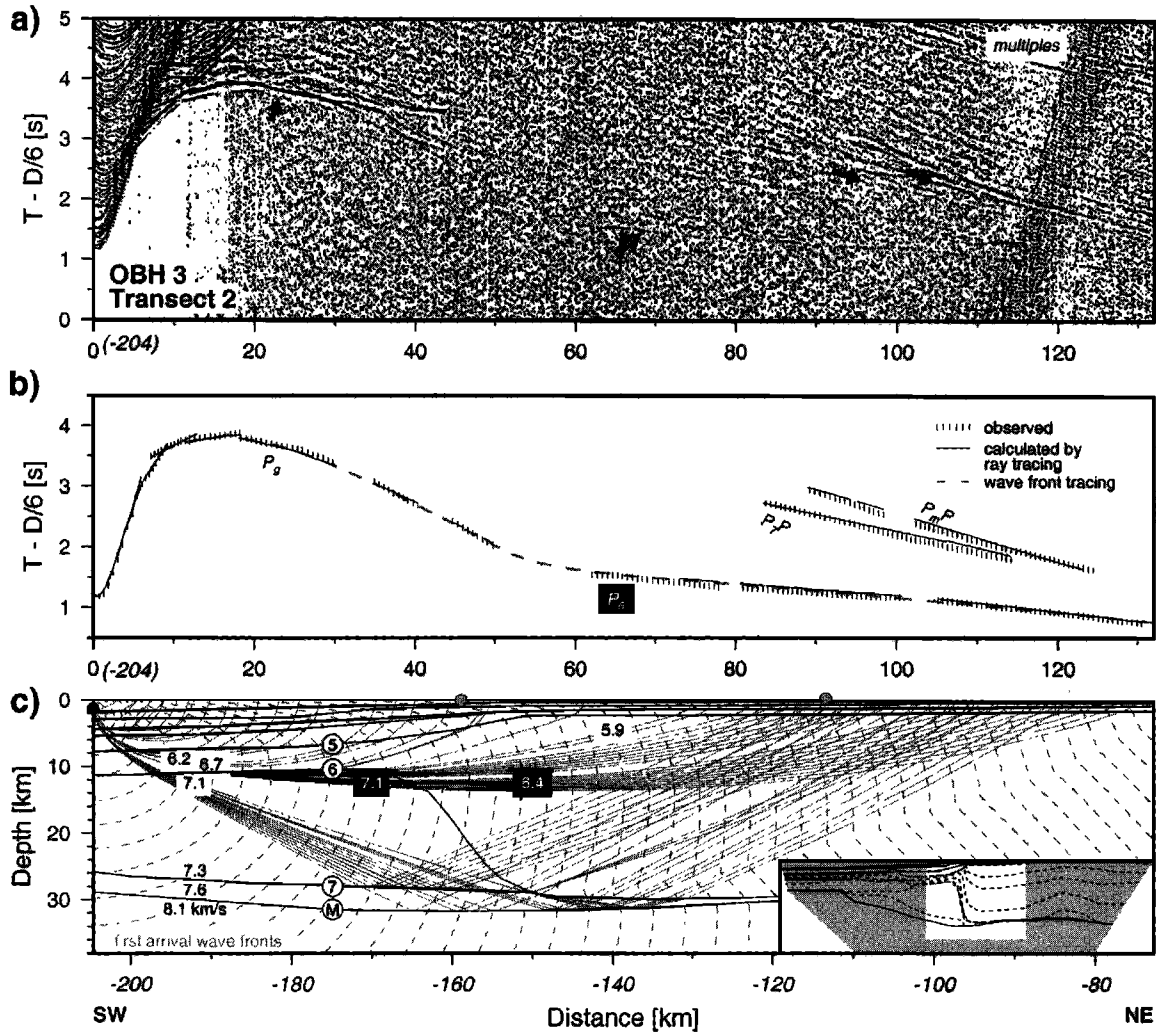


**Figure 10.** Seismic data recorded by OBH 3 on transect 2. The data are displayed as in Figure 4. Theoretical travel times were calculated for the final  $P$  velocity model (Plate 1b).

served at different land stations on this transect, at -15 km a high-velocity anomaly of up to +0.5 km/s with respect to the surrounding material was modeled. This feature is necessary to fit the early arrivals on the one hand and the apparent velocity of  $\sim 5.9$  km/s characterizing  $P_5$  on the other hand. The enlarged details in Figures 8 a and b illustrate the significance of this model feature because the theoretical  $P_5$  arrivals are predicted several wavelength later than the observed arrivals if the high-velocity region is not included in the model. The  $P_6$  arrivals at offsets between -155 and -180 km were modeled as refractions from the high-velocity zone beneath boundary 6 ( $> 7.1$  km/s) and confirm the OBH data modeling. The Moho could be constrained by  $P_mP$  reflections. Refracted arrivals from the uppermost mantle ( $P_n$ ) are very weak, which is probably due to a very small or even negative velocity gradient beneath the Moho.

The ray coverage 9) and travel time fitting for transect 2 (Figure is similar to that of transect 1. Figure

10 shows data from OBH 3 on transect 2. We observe irregular  $P_5$  travel time branches at offsets between 30 and 120 km. The significant change in apparent velocities is due the seafloor and basement topography as well as to a strong lateral velocity gradient in the entire crust at about -160 km (see COB in Plate 1b). Clear  $P_mP$  reflections define the Moho boundary. The land data on transect 2 (e.g. Figure 11) show  $P_5$  arrivals which can also be traced as secondary phase at larger offsets. This gives important control on the middle and lower crustal velocities and supports the model of a strong lateral velocity gradient at about -150 km. In contrast to the land data on transect 1, clear  $P_n$  arrivals are recognizable in transect 2.

### 3.2. Seismics and Gravity

Rifted continental margins are characterized by prominent free-air gravity anomalies elongated parallel to the ocean-continent transition [e.g., Rabinowitz and LaBrecque, 1979; Holbrook et al., 1994b; Watts and

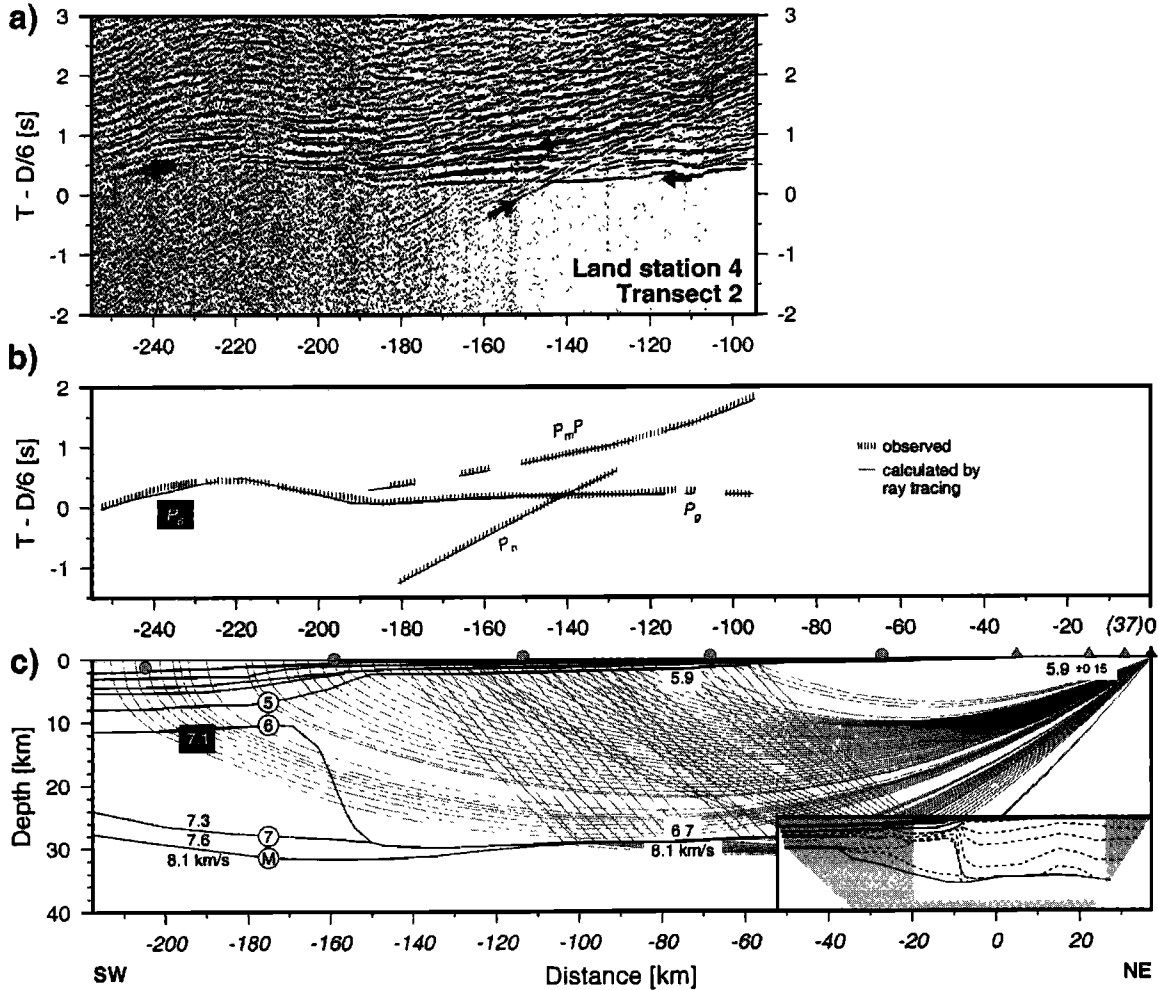


**Figure 11.** Receiver gather comprising vertical component recordings of land station 4 on transect 2. The data are displayed as in Figure 4. Theoretical travel times were calculated for the final  $P$  velocity model (Plate 1b).

[*Fairhead*, 1999]. The cause of these anomalies is not always clear because of the ambiguity inherent in potential field data interpretation. In this section we attempt to explain the gravity anomalies in the study area by use of the seismic information on crustal structure and velocity.

The gravity data compiled for the region of transects 1 and 2 (Figure 12) reveal a prominent positive anomaly parallel to the shelf break. This feature is observed along large portions of the Atlantic margins [*Watts and Fairhead*, 1999] and is accompanied by a seaward gravity low in some cases. *Sleep and Fuyita* [1997] demonstrated that a simplified ocean-continent transition (oceanic crust bordering directly on continental crust, both of uniform thickness and isostatically compensated) produces an antisymmetric free-air anomaly located at this boundary with a high on the outer shelf and a low on the oceanic crustal edge. In nature, such a transition of crustal blocks is much more complex and local disturbances of isostasy are probable because of the rigidity of the brittle parts of the lithosphere. Free-air gravity is very sensitive to such

complexity [*Watts and Fairhead*, 1999] and the idealized edge effect is distorted in many cases.

*Rabinowitz and LaBrecque* [1979] interpreted the shelf anomaly off southwest Africa as such an edge effect produced by the juxtaposition of continental and oceanic crust. Their study, however, lacked control from deep seismic data. Whereas later studies [e.g., *Light et al.*, 1992; *Gladchenko et al.*, 1998] have not agreed with the edge effect interpretation, our velocity models do show a major crustal boundary at the position of the gravity high (see COB in Plate 1 and Figure 12). Thus, in the following discussion we refer to this as the COB edge effect anomaly. An outer gravity high is more diffuse and of smaller amplitude, but it can be traced parallel to the margin into the southern Cape Basin. This feature correlates approximately with the TNOB boundary in Plate 1. We interpret this as a similar edge effect (TNOB edge effect). Furthermore, gravity data show a circular high at the position of the Cape Cross intrusive complex, which appears to support the  $P$  velocity model of a vertical structure with enhanced seismic velocity at this location (Plate 1).

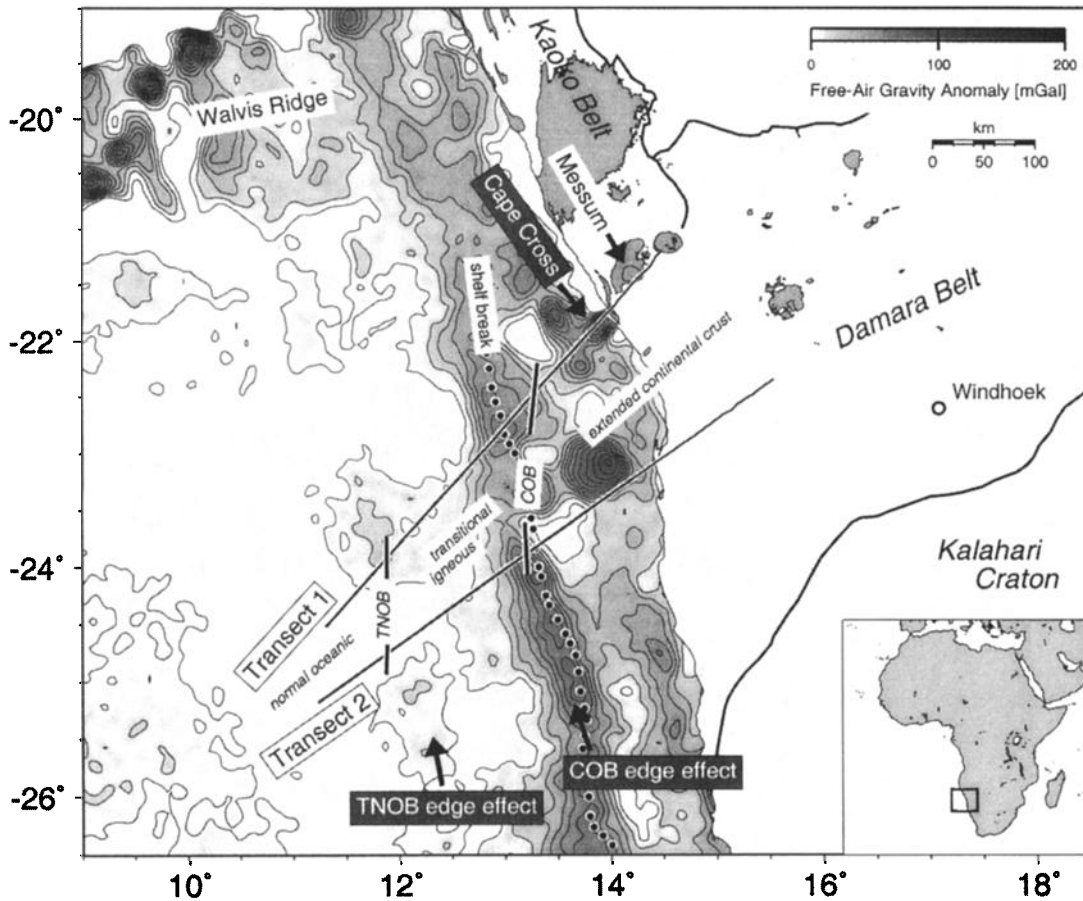


**Figure 12.** Free-air gravity anomaly map for the region of this study (compiled from Sandwell and Smith [1997]). Superimposed are interpretative zonations along transects 1 and 2 (see Plate 1, COB, continent-ocean boundary; TNOB, transitional-normal oceanic crustal boundary). Shelf break is from bathymetry of Wessel and Smith [1991]. Simplified onshore geology of the Damara orogeny and Mesozoic igneous complexes is displayed as in Figure 2.

We tested these tentative interpretations by calculating the gravity response of our crustal model along transect 1 and comparing the results with the observed data. The crustal densities were calculated from the velocity model using velocity-density relations from global studies of Ludwig *et al.* [1970] for sedimentary rocks and Christensen and Mooney [1995] for igneous and metamorphic rocks (Figure 13). Whereas seismic modeling using ray tracing involves a geometric model that is parameterized by layers with linear velocity gradients, the general basis for gravity modeling is a distribution of bodies with homogeneous density [Talwani *et al.*, 1959]. The common approach, whereby seismic velocity layers are converted into polygons with homogeneous density, would not result in a truly equivalent density model in our case because of the strong lateral and vertical velocity gradients of the model. To get around this problem, the velocity model was densely gridded (cells of 0.5 by 0.05 km, width by height), and the density of each cell was determined using the function shown in Figure 13. To avoid artificial side effects, the grid cells at

the edges of the model were extended laterally several hundred kilometers. The theoretical gravity response of the model was obtained by superposition of all single-cell effects, calculated by the formulae of Talwani *et al.* [1959] [see Sleep and Fuyita, 1997].

Without any changes to the model derived from seismic data alone, the agreement of calculated with observed gravity is already satisfying except for the Cape Cross anomaly (Figure 14). To fit this feature some changes in the velocity model were applied within the range of the velocity uncertainties (see Plate 1a and Figure 14b), and this led to a reasonable fit between measured and predicted gravity. Supposing the general validity of the velocity-density relation that was used here, these adjustments imply that the high-velocity zone underneath the Cape Cross anomaly is, in fact, underestimated by the seismic modeling and that there must also be higher velocities in the seismically poorly resolved lower crust. Alternatively, there could be a deviation from the general velocity-density correlation for the material within this zone. These arguments remain

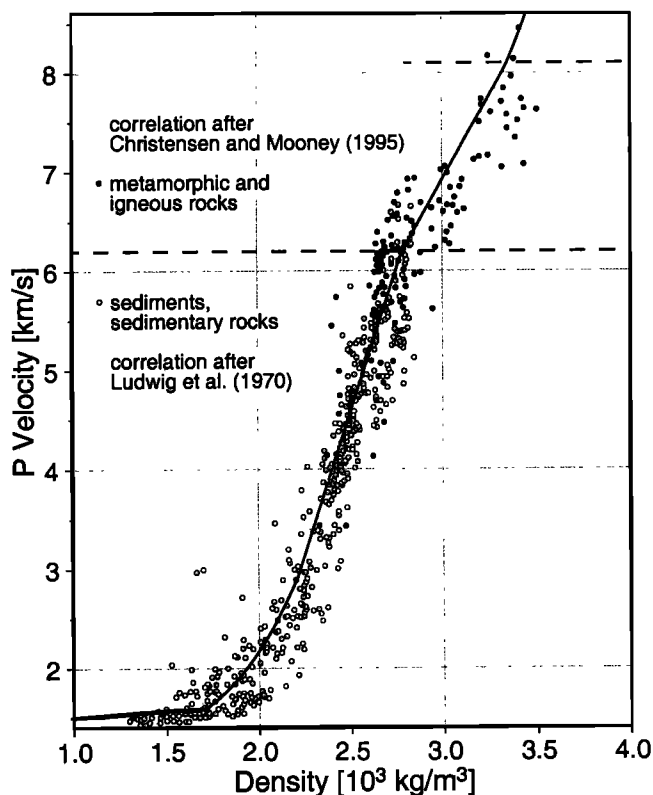


**Figure 13.** Conversion of the  $P$  velocity model into a grid-based density field. The velocity-density function is composed of a curve branch for sedimentary rocks (Nafe-Drake curve [Ludwig et al., 1970]) and from correlations for igneous and metamorphic rocks [Christensen and Mooney, 1995].

valid if we take into account the error from using 2-D instead of 3-D modeling because even higher densities would be necessary to explain the anomaly.

The cause of the gravity anomalies, which correlate with the crustal boundaries COB and TNOB, was investigated by perturbation of relevant parameters of the model. The anomaly near the COB is produced by superposition of topography effects and lateral density variations. The maximum at about -150 km coincides with the shelf break. However, the width and amplitude of this anomaly also require dense material in the middle and lower crust. This provides further support for the existence of a high-velocity zone in this region. The abrupt lateral change in crustal densities (velocities) is responsible for the landward termination of the anomaly.

The gravity anomaly approaches zero on both sides of the TNOB. This results from the superposition of competing factors. Whereas the landward decreasing water depth and increasing crustal density contribute with a landward increase of gravity, the landward deepening of the Moho contributes a gravity decrease. The crustal blocks east and west of the TNOB differ with respect to these lateral changes, and the result is a gravity high at their border. We conclude that both the anomalies near

the COB and TNOB are edge effects caused by the presence of the high-velocity (density) lower crustal body and its juxtaposition with the landward and oceanward crustal blocks, respectively.

### 3.3. Magnetics

Magnetic total intensity data were acquired along both transects using a shipborne proton magnetometer. Magnetic anomalies were calculated from the total field data through removal of the IGRF95 reference field [IAGA Division V, Working Group 8, 1996]. The resulting anomalies are displayed in Figure 2 as wiggle traces along the profile lines. Owing to the lack of a magnetic reference station, no further corrections were applied. At least for the magnetic anomalies on transect 2, which are interpreted below in some detail, we are sure that the data are not significantly influenced by magnetic variations because the line was surveyed twice from opposite directions. The only difference between both anomaly curves is a long-wavelength deviation of up to 20 nT that does not influence the modeling and interpretation.

Near the coast, both transects show magnetic anomalies of high amplitude and short wavelength, which are presumably caused by mafic volcanic rocks present at shallow depths in the shelf area. Farther seaward on these lines we observe high-amplitude, long-wavelength, mostly positive magnetic anomalies, which correspond in part with the location of SDR wedges and other features of the seismic sections. These are best displayed on transect 2 and are discussed in detail below.

Our transects cross the magnetic lineations identified by Rabinowitz and LaBrecque [1979] as seafloor-spreading anomalies M4 and M2. A single prominent positive anomaly on the southwest part of transect 2 may correspond to the M4 anomaly, but there is no similar anomaly in the appropriate position on transect 1. Anomaly M2 also does not show up distinctly in our data, and we therefore can neither confirm nor deny the identification of the magnetic lineations shown in Figure 2.

The most prominent positive long-wavelength anomaly on transect 2 (reaching ~500 nT) is located near the position of anomaly G on existing maps. This anomaly was first recognized by Larson and Ladd [1973] and was later mapped in more detail by Rabinowitz and LaBrecque [1979]. Rabinowitz and LaBrecque [1979] fixed anomaly G at the landward end of the broad positive anomaly or at a magnetic minimum that sometimes accompanies the broad positive anomaly. The location of anomaly G in later publications and shown in our Figure 2 is based on this definition. Anomaly G was interpreted by Rabinowitz and LaBrecque [1979] as an edge effect caused by different magnetic properties of oceanic and continental crust and was used as a marker for the COB. However, alternative explanations have been offered and the cause of the G anomaly is still

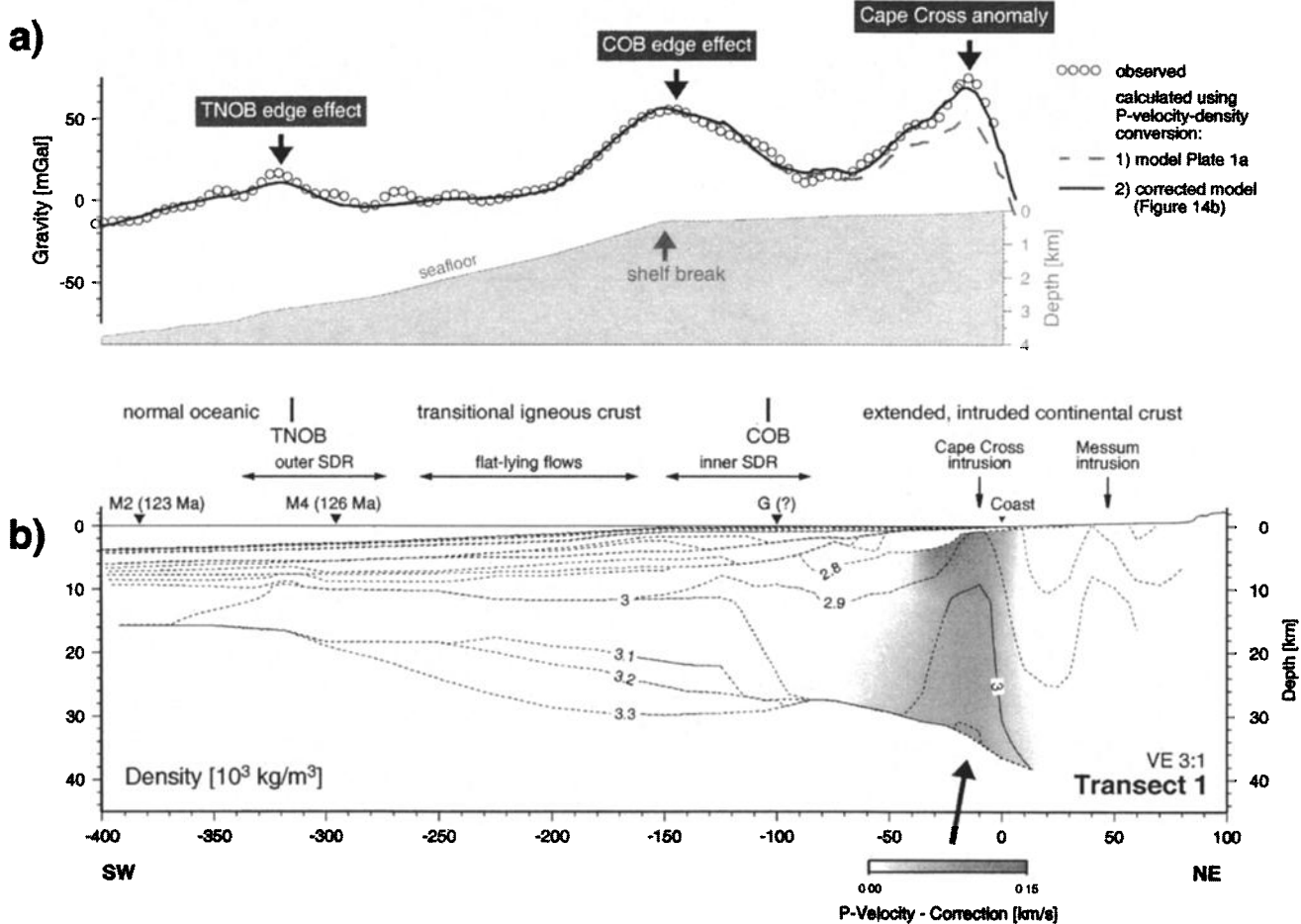


**Figure 14.** (a) Calculated and observed free-air gravity anomalies. Velocity-density conversion was used as shown in Figure 13. Curve 1 shows resulting gravity for the velocity model shown in Plate 1a. Curve 2 was calculated after some corrections in the velocity model (see below). (b) Density model for transect 1 with velocity corrections.

controversial. For example, *Hinz et al.* [1999] suggested that anomaly G off Argentina is caused by thick layers of extrusive basalts that can be identified as SDRs in reflection seismic sections.

On our new magnetic data we define anomaly G by its most striking feature, a zone of mostly positive amplitude enhancement  $\sim$ 50–100 km wide, which may be overlain by short-wavelength anomalies. The fact that anomaly G, particularly on transect 2, corresponds in position with the inner wedge of SDRs suggests that it may be caused by near-surface lithologies and not by a throughgoing crustal boundary as implied by the edge effect hypothesis. To test the significance of the anomaly G in the present study area, we performed forward modeling of the magnetic anomalies on transect 2 using geometrical constraints derived from the reflection and refraction seismic data. The most prominent feature in the model (Figure 15) is a 4 A/m remanent magnetic body which corresponds approximately with the location and shape of the inner SDR wedge. Our interpretation of anomaly G as mainly due to the

inner SDR wedge is consistent with data from other volcanic margins, e.g., the Vøring Plateau in the North Atlantic [*Schreckenberger*, 1997]. Drilling results from Ocean Drilling Program (ODP) Leg 104 on the Vøring Plateau [*Schönharting and Abrahamsen*, 1989] indicate high remanent magnetization values for the SDRs that makes them a preferred candidate for the volcanic passive margin anomalies. The contribution of a deep-source crustal contrast (edge effect) is not required to explain the magnetic data, although it cannot be discounted. However, we favor an explanation based on source bodies with proven magnetic properties instead of others for which we can only speculate about their magnetic properties.

We attribute the negative anomaly landward of the inner SDR wedge to basaltic flows of similar character but having reversed magnetization ( $-4$  A/m). This implies a reversal of the Earth's magnetic field between the time of emplacement of the inferred landward flows and of the inner SDR wedge. The model for much of the zone of flat-lying flows seaward of the inner wedge

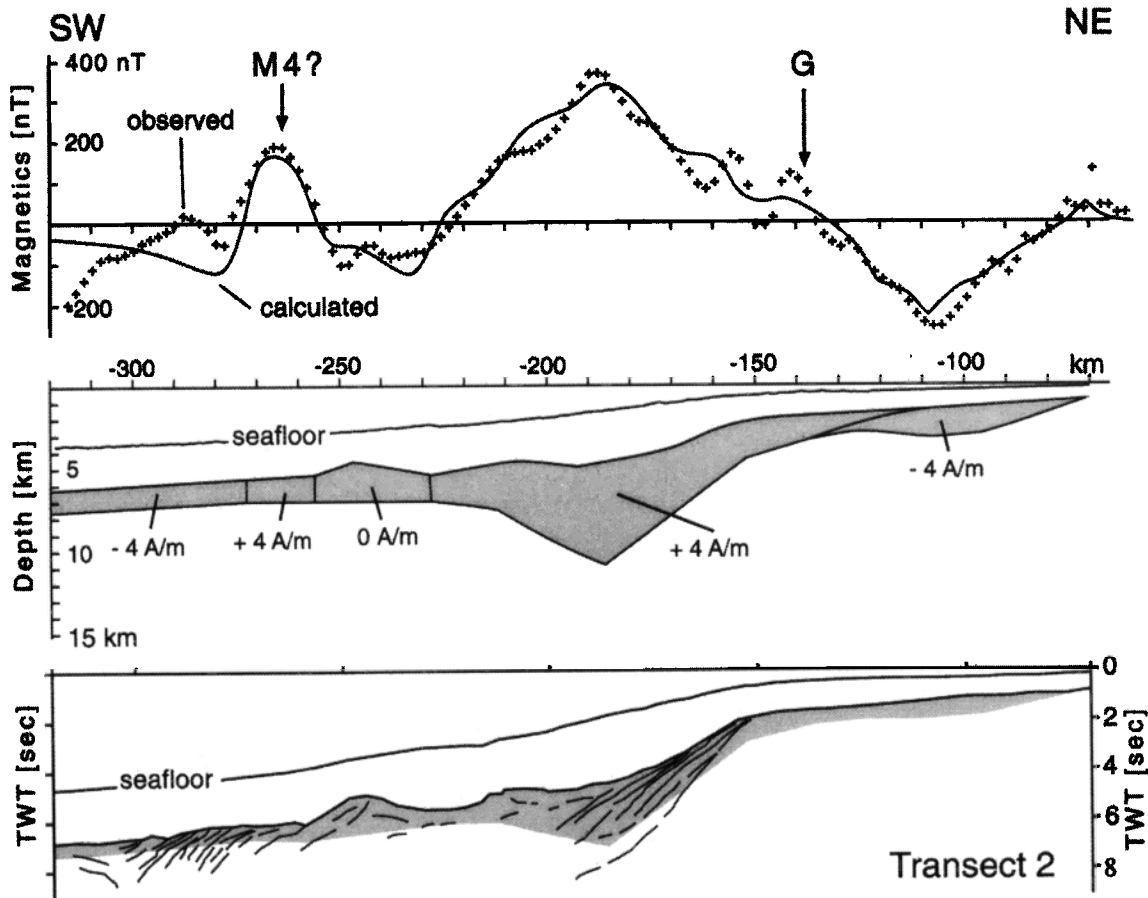


**Figure 15.** Two-dimensional magnetic model calculation for transect 2. The model body from the middle panel (depth scale) was converted into the travel time scale of the line drawing (shaded area in the bottom panel) using an average  $P$  velocity of 5 km/s. Magnetization labels denote remanent magnetization intensities. Direction of remanence (inclination;  $-57^\circ$ ; declination;  $-33^\circ$ ) according to the paleopole position for Africa in the Early Cretaceous [Van der Voo, 1993]. Negative remanence denotes reversed magnetization. Every source body has an additional induced magnetization component of 1.5 A/m [Schreckenberger, 1997].

of SDRs (-230 to -255 km) suggests a body with no net remanent magnetization. A possible explanation for this would be that flows with opposing polarity were emplaced on top of each other during a period of frequent reversals of the Earth's magnetic field. Magnetic timescales [e.g., Harland et al., 1990] show an interval of frequent reversals (M5 to M9) over a time span of  $\sim 2$  Myr predating M4. This process would cancel out the effect of remanent magnetization and leave only the induced component. West of -255 km the model assumes an average magnetization of normal oceanic crust with a polarity reversal at -270 km, which might represent the boundary between the inverse polarity interval M3 and the normal interval M4.

The inferred polarity of modeled magnetic anomalies offers the potential of constraining the timing of magmatism on the Namibian margin. The width of the normal magnetic interval on transect 2, which is correlated tentatively as M4, corresponds to a spreading rate of 2 cm/yr, in good agreement with Rabinowitz and

LaBrecque [1979], who modeled the southwest African spreading anomalies using 1.5 cm/yr. Emplacement of the normal-polarity inner wedge of SDRs might have happened during the 2-Myr period including M10 and partly M11, which was dominated by a normal field. This corresponds well to the peak age of flood basalts volcanism on land (134–130 Ma [Milner et al., 1995; Renne et al., 1996]). However, we consider it unlikely that good constraints on spreading rate and emplacement ages can be derived from the magnetic response of SDR wedges because it is generally assumed that they were emplaced at high accumulation rates through intensive pulses of magmatism [e.g., Schönharting and Abrahamsen, 1989].

#### 4. Interpretation and Discussion

Both margin transects reveal similar characteristics of the crust across the ocean-continent transition. The following discussion is therefore organized according to the

general features common to both transects: (1) postrift sediments, (2) normal oceanic crust, (3) transitional igneous crust, and (4) extended continental crust:

#### 4.1. Postrift Sediments

The nature of the seismic sequence between the seafloor and the acoustic basement B along the transects 1 and 2 (Figures 3–5) are in good agreement with the results of previous MCS surveys in this region. These studies related horizon L [Gerrard and Smith, 1982; Light et al., 1992] (named D by Austin and Uchupi [1982]) with an erosional surface at the base of the Tertiary. This interpretation was confirmed by drilling in the southern Cape Basin [Bolli et al., 1978] and was extrapolated into the northern Cape Basin [Austin and Uchupi, 1982], including the area of our study. Following this interpretation, horizon L on our transects separates lower Eocene calcareous ooze and mud from upper Paleocene carbonate-poor clays [Bolli et al., 1978]. The seismic  $P$  velocities determined from our wide-angle data are  $\sim 1.7\text{--}2.1$  km/s in the upper layer and  $2.4\text{--}2.8$  km/s in the layer beneath horizon L, which support the lithological interpretation referenced above, considering the broad range of sedimentary rock velocities [e.g., Schön, 1996]. The strong vertical gradient of  $P$  velocities could be related to compaction and decrease of pore space with depth caused by increasing overburden.

The second prominent discontinuity in the seismic sections above the acoustic basement can only be identified at the lower continental rise and at the continental slope. This horizon N correlates with that of previous surveys [Gerrard and Smith, 1982; Light et al., 1992] (equivalent to AII of Austin and Uchupi [1982]). It was interpreted as an erosional surface. Well control in the Cape Basin showed that it separates Upper Cretaceous shales and turbidites from Lower Cretaceous sandy mudstones and sandstones. Our seismic  $P$  velocities in this zone support this interpretation, with values of 2.8 km/s above and 4.0–4.4 km/s beneath horizon N being reasonable for such sedimentary rocks [Schön, 1996]. No further seismic boundaries were identified above the acoustic basement B. We interpret the sequence from the seafloor to horizon N as drift sediments of open-water marine facies with minor terrigenous input in a subsiding marginal basin. The sequence below horizon N could represent mainly terrigenous sediments, which were deposited during faster initial subsidence.

#### 4.2. Normal Oceanic Crust

The SW ends of both transects have basement  $P$  velocities and Moho depths and crustal thicknesses typical for oceanic crust produced under standard seafloor spreading conditions. The acoustic basement reflector B probably represents the top of the basaltic layer 2, with reasonable  $P$  velocities for oceanic basalts between 4.8 and 5.5 km/s [Detrick et al., 1994]. The crust below this layer has  $P$  velocities increasing with depth from

6.1 km/s at the top to 7.1 km/s at the base, suggesting gabbroic material consistent with oceanic layer 3 [e.g., Detrick et al., 1994]. The total thickness of oceanic basement (between basement reflector B and the Moho) reaches 8 to 9 km, which is greater than on average and could point to slightly higher melting rates during initial seafloor spreading. A similar finding was reported from seismic surveys off the U.S. East Coast by Holbrook et al. [1994a].

#### 4.3. Transitional Igneous Crust

One of the most important results of our integrated wide-angle and reflection seismic modeling is the new insights gained on the nature of the ocean-continent transition zone. Whereas previous studies of Austin and Uchupi [1982], Light et al. [1992], and Gladzenko et al. [1997] discuss the transition zone in terms of rifted relict crust, we suggest that the reflectivity images,  $P$  velocities, densities, and magnetic features are consistent with the interpretation that the crust in this region consists almost exclusively of igneous material. This interpretation relies mainly on the nature of the two SDR wedges flanking the transition zone and of the underlying middle and lower crust, and it is therefore necessary to describe these in some detail.

Both SDR wedges, as well as the intervening flat reflectors (flows) and mound-like structures, and the reflectors (flows) beneath the shelf correlate seaward with the oceanic layer 2. Apart from this geometric correlation, a similar basaltic composition for these features is indicated by the fact that  $P$  velocities (4.8–5.5 km/s) in this layer vary only slightly and are in a typical range for extrusive basalts [Detrick et al., 1994]. The succession of extrusive complexes inferred from our transects has also been identified by seismic studies on the Norwegian and western Australian volcanic margins [Planke et al., 1999]. They explain the distinct reflection seismic characteristics of the extrusive units by different emplacement environments and volcanic facies. According to their scheme the outer wedge is probably related to deep marine flood and pillow basalt flows, followed landward by shallow marine hydroclastic flows and mounds. The inner SDR wedge and its flat-dipping continuation beneath the shelf are supposed to represent flood basalts and intercalated sediments emplaced under subaerial conditions. This is the type of rock sequence encountered by the Deep Sea Drilling Project (DSDP)/ODP drill holes that have penetrated (inner) SDR wedges so far (Hatton Bank margin [Roberts et al., 1984]; Voring Plateau [Eldholm et al., 1987]; and SE Greenland [Larsen et al., 1994]).

The magnetic modeling discussed above provides further support for these interpretations. The value of 4 A/m for the remanent magnetization of the inner SDR wedge fits the observed magnetic anomalies and lies within the range of values that are typical for extrusive basalts [Schreckenberger, 1997]. Our interpretation that the wedge consists of basalt flows and intercalated sedi-

ments deposited under subaerial conditions is supported by Schreckenberger [1997], who showed that this type of volcanic sequence is prone to acquisition of strong magnetic remanence comparable in magnitude to that of oceanic pillow basalts. The lack of a magnetic anomaly corresponding to the outer SDR wedge is surprising. We suggest that the basalts of the outer wedge were emplaced under subaqueous conditions and have magnetic properties which resemble those of normal oceanic crust.

The crust beneath the zone of SDR wedges and basaltic units is characterized by high average  $P$  velocities ( $>7$  km/s), which can only be explained by igneous composition [Schön, 1996]. It seems plausible that the crust underneath the SDR wedges and flow structures represents the intrusive counterpart of the overlying extrusives. Similar crustal sections have been reported from volcanic margins in the North Atlantic, including the Hatton Bank margin [White et al., 1987] and the U.S. Atlantic margin [Holbrook et al., 1994a, b]. This type of ocean-continent transition is commonly interpreted as a zone of extended and rifted continental crust which is heavily intruded and underplated by mafic magmas [White et al., 1987]. However, Holbrook et al. [1994b] noted the lack of direct evidence for continental crust in such zones. Indeed, our data from the Namibian margin show no typical rift-related structures such as rotated blocks, although these could be masked by the strongly attenuating sediments and basalts or overprinted by magmatic intrusions. While we cannot exclude the interpretation of the crustal  $P$  velocities beneath the extrusive section as heavily intruded, extended continental crust, we favor an explanation similar to that of Holbrook et al. [1994b] that this zone consists of completely accreted igneous material. Support for this model comes from the strong lateral velocity gradient landward of the inner SDR wedge, which extends to shallow crustal levels. This could represent the landward termination of the intrusive section. Its transition to normal oceanic crust on the seaward side appears much more gradual.

This interpretation of the COB as new igneous crust implies the formation of the Namibia volcanic margin by relatively abrupt continental rupture over a narrow rift zone in contrast to the formation of a wide zone of extended and intruded continental crust. In both cases, but particularly if the high-velocity body represents entirely igneous material, the amounts of partial melts produced during continental breakup are much larger than during normal seafloor spreading. White and McKenzie [1989] showed that the amount of decompressional melting depends on the potential temperature of the asthenosphere and on the timing and degree of lithospheric thinning. Apart from the anomalous thickness of igneous crust in the transition zone, the high seismic velocities of the lower section in this zone suggest distinctly denser material than would be typical for mid-ocean ridge basalt (MORB)-like rocks

and this in turn suggests a greater than normal degree of melting. Petrophysical modeling of the high-velocity crust underneath boundary 6 (Plate 1) by Sobolev et al. [1998] showed that the  $P$  velocities are appropriate for olivine-rich high-Mg magmas, which require  $>20\text{--}25\%$  partial melting of peridotite and a higher than normal potential temperature of the mantle [see also Farretni et al., 1996].  $P$  wave velocities of  $\sim 7.6$  km/s at the base of this crustal section could represent an interlayered gabbro-dunite transition zone [Canales et al., 2000]. The seismic Moho corresponds to the base of this body and represents the transition to normal peridotitic mantle.

#### 4.4. Continental Crust

The continental crust landward of the COB shows striking differences in velocity structure and Moho depth between transects 1 and 2 (Plate 1) which reflect differences in the regional geology. The crust on transect 2 has a uniform velocity structure with similar values as derived for the southern central zone of the Damara Belt [Baier et al., 1983; Green, 1983]. Transect 1 crosses two major Cretaceous intrusive complexes (Messum and Cape Cross), and the velocity structure shows high-velocity anomalies beneath them that extend through the entire section (Plate 1 and Figure 14). The high-velocity anomaly beneath the Messum intrusion most likely reflects intracrustal intrusions of gabbroic material, which fed the Messum igneous system. Geochemical and isotopic data from the Messum gabbros indicate a mantle source for the basic magmas [Ewart et al., 1998]. Therefore it is not surprising that the high-velocity anomaly beneath the Messum intrusion extends through the entire crust. The Cape Cross complex is mostly submerged beneath the sea, but its extent offshore is indicated by a positive gravity anomaly (Figure 14). This and the similarity in velocity structure beneath Cape Cross and Messum suggest that a mafic root of comparable size exists beneath both complexes.

The cause of reflectivity of the lower continental crust such as we observe on transect 1 is controversial. Prominent end-member models are layering of mafic igneous intrusions (sills) associated with intense magmatic activity and ductile stretching of heterogeneous crust in an extensional regime [e.g., Meissner and Brown, 1991]. The lower crustal reflectivity seaward of the Cape Cross intrusion is likely to be caused by mafic sills associated with the intrusive complex. The wide-angle data reveal midcrustal reflections from the top of this reflective zone, but there is no evidence for a discontinuous increase of velocity at this boundary. However, Holliger and Levander [1994] have shown that lithologic diversity in the lower crust resulting from mafic intrusions can produce lower crustal reflectivity without a discontinuous change of the large-scale velocity structure at the top of this zone. The apparent gap in the midcrustal floating reflector underneath the Cape Cross complex

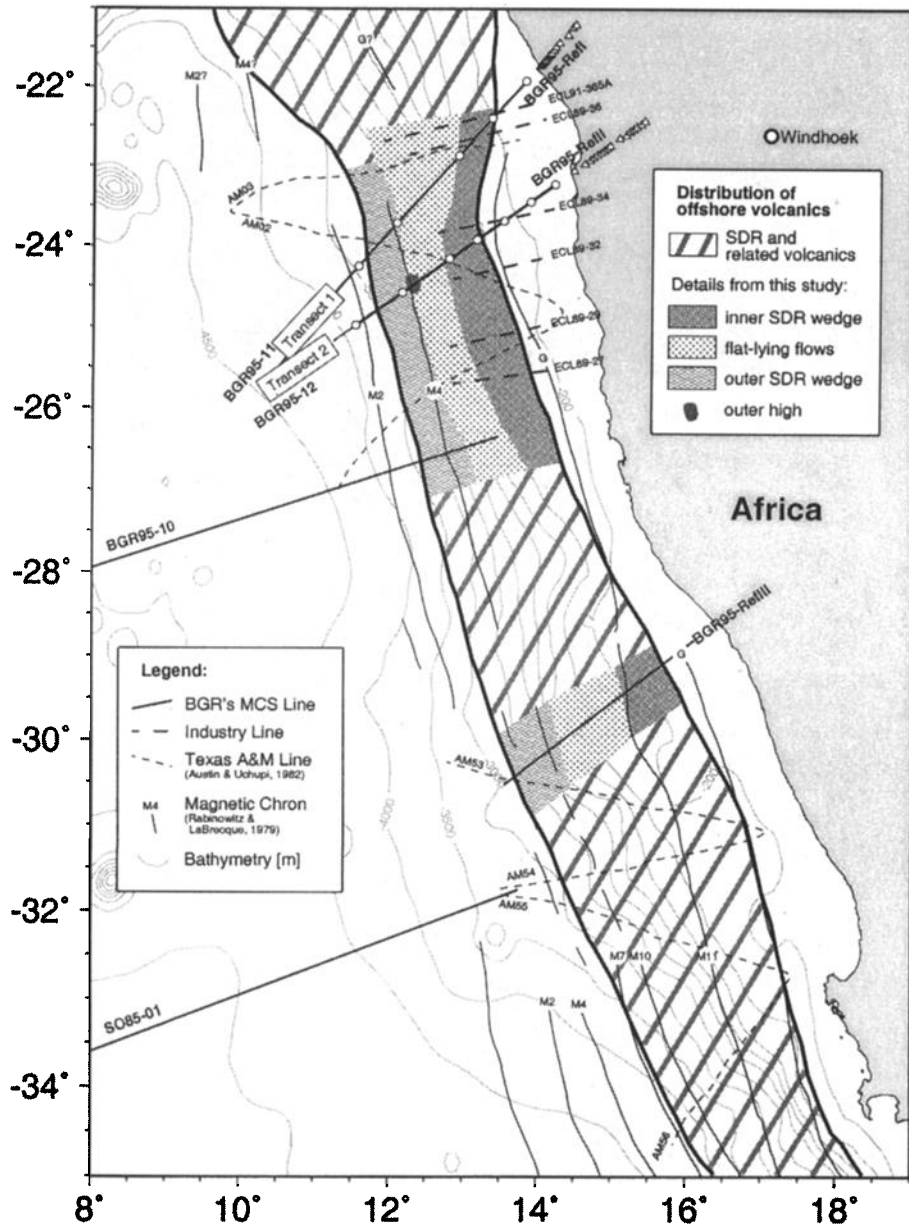


**Figure 16.** Distribution of breakup-related volcanics offshore Namibia. The map summarizes the interpretations of this study and those from former reflection seismic surveys.

may indicate that intrusions are vertically oriented under and within the complex itself. The lack of lower crustal reflectivity at the COB may reflect the onset of entirely oceanic crust, or it may result from strong attenuation of energy due to the overlying basaltic SDR wedge. Both explanations support the interpretation of this transition as the COB. The lower crustal reflectivity is lacking on transect 2, probably because magmatism was much weaker in that region.

The Moho depth at the coast is  $\sim 35$  km on transect 1 and  $\sim 29$  km on transect 2. This difference can be attributed to their positions in the Damara Orogen. Whereas transect 2 is located in the central zone of the Damara Belt, transect 1 crosses the juncture between

the Damara Belt and the Kaoko Belt (Figure 2), and the greater crustal thickness at this position may result from the combined effect of the east vergent Kaoko compression and the north vergent Damara Belt.

## 5. Conclusions

We have presented new geophysical data, which were collected along two traverses across the continental margin of Namibia. Two wedges of seaward dipping reflectors (inner and outer SDRs) were identified at  $\sim 100$ - $150$  km and  $300$  km offshore. We infer from integrated modeling and interpretation of seismic and potential field data that these units and intervening structures

are basaltic. The crust underlying the SDR zones is characterized by high velocities and densities (average of  $\sim 7 \text{ km s}^{-1}$ ,  $3 \times 10^3 \text{ kg m}^{-3}$ ) that can be explained only by igneous material. Our data show no evidence for rift-related tectonism in this zone. We conclude that the inner and outer SDRs flank a zone of exclusively igneous crust with unusual thickness (up to 25 km). This zone shows a gradual transition into normal oceanic crust seaward, whereas its landward termination is marked by an abrupt lateral decrease of the velocities and densities in the entire crust. We define the continent-ocean boundary (COB) as the landward velocity transition, and consequently, the thick high-velocity crust seaward of the COB is interpreted as exclusively igneous material and not intruded continental crust.

A key to the understanding of volcanic margin formation is the ability to map breakup-related magmatic features along the continental margin. The integrated interpretation of various geophysical data sets allows a certain degree of extrapolation of structures along the southwestern African margin. The distribution of seaward dipping reflectors along the Namibian margin (Figure 16) marks, in our opinion, the zone of thick, high-velocity igneous crust. Our interpretation of free-air gravity anomalies on the landward and seaward sides of this zone as edge effects gives additional support for the continuation of the high-velocity zone along the margin farther south. An observation consistent with this interpretation is that both the seaward dipping reflectors and comparable gravity anomalies are lacking north of the Walvis Ridge [Sibuet *et al.*, 1984; Gladchenko *et al.*, 1998]. Finally, because the long-wavelength magnetic anomaly G is related with the inner SDR wedge, it is also considered a reasonable marker of the COB on this margin.

We propose from the interpretations of crustal transects 1 and 2 and the extrapolation of related geophysical features farther south that thick igneous crust formed along the entire margin south of the Walvis Ridge. As suggested by Sobolev *et al.* [1998], the enhanced mantle potential temperatures required to produce the inferred high-Mg magma composition of thick igneous crust can be reasonably explained as a result of the Tristan da Cunha mantle plume. The influence of the mantle plume is further suggested by the widening of the thick igneous crust near the Walvis Ridge (compare transects 1 and 2). However, the apparent continuation of thick igneous crust at the COB farther to the south could indicate that the breakup process itself stimulates passive enhanced convection at the continental edge.

**Acknowledgments.** The Geological Survey of Namibia (GSN) and the German Mineral Prospecting Promotion Project (BGR and GSN) supported the surveying on land. Special thanks to Bodo Baier, Jens Bribach, Detlef Eberle, Jürgen Oswald, Trond Ryberg, Alexandra Speiser, and Rainer Wackerle. Heinrich Meyer and Christian Reichert conducted the seismic surveys offshore. The equipment

for the measurements on land was provided by the Geophysical Instrument Pool Potsdam (GIPP) at the GFZ. We thank Colin Zelt for making available Rayinvr. Michael Roth kindly provided the finite difference travel time modeling program. Figures have been generated with the GMT software of Wessel and Smith [1991]. Reviews by Walter Mooney, Vera Schlindwein, and Uri ten Brink helped to improve the manuscript. Funding was provided by BGR, AWI, and GFZ.

## References

- Arndt, N. T., and U. Christensen, The role of lithospheric mantle in continental flood volcanism; thermal and geochemical constraints, *J. Geophys. Res.*, **97**, 10,967–10,981, 1992.
- Austin, J. A., and E. Uchupi, Continental-oceanic crustal transition off Southwest Africa, *AAPG Bull.*, **64**, 501–526, 1982.
- Baier, B., H. Berckhemer, D. Gajewski, R. W. Green, C. Grimsel, C. Prodehl, and R. Vees, Deep seismic sounding in the area of the Damara Orogen, Namibia, southwest Africa, in *Intracontinental Fold Belts*, edited by H. Martin and F. Eder, pp. 885–900, Springer-Verlag, New York, 1983.
- Bolli, H. M., et al., Cape Basin continental rise; Sites 360 and 361, *Initial Rep. Deep Sea Drill. Proj.*, **40**, 29–182, 1978.
- Brown, R. W., D. J. Rust, M. A. Summerfield, A. J. W. Gleadow, and M. C. J. DeWit, An early Cretaceous phase of accelerated erosion on the south-western margin of Africa: Evidence from apatite fission track analysis and the offshore sedimentary record, *Nucl. Tracks Radiat. Meas.*, **17**, 339–350, 1990.
- Canales, J. P., R. S. Detrick, J. Lin, and J. A. Collins, Crustal and upper mantle seismic structure beneath the rift mountains and across a nontransform offset at the Mid-Atlantic Ridge ( $35^\circ\text{N}$ ), *J. Geophys. Res.*, **105**, 2699–2719, 2000.
- Christensen, N. I., and W. D. Mooney, Seismic velocity structure and composition of the continental crust: A Global Review, *J. Geophys. Res.*, **100**, 9761–9788, 1995.
- Coffin, M. F., and O. Eldholm, Large igneous provinces: Crustal structure, dimensions, and external consequences, *Rev. Geophys.*, **32**, 1–36, 1994.
- Detrick, R., J. Collins, R. Stephen, and S. Swift, In situ evidence for the nature of the seismic layer 2/3 boundary in the oceanic crust, *Nature*, **370**, 288–290, 1994.
- Duncan, R. A., P. R. Hooper, J. Rehacek, J. S. Marsh, and A. R. Duncan, The timing and duration of the Karoo igneous event, southern Gondwana, *J. Geophys. Res.*, **102**, 18,127–18,138, 1997.
- Eberle, D., D. G. Hutchins, R. J. Rebbeck, and I. Somerton, Compilation of the Namibian airborne magnetic surveys: Procedures, problems and results, *J. Afr. Earth Sci.*, **22**, 191–205, 1996.
- Eldholm, O., and K. Grue, North Atlantic volcanic margins: Dimensions and production rates, *J. Geophys. Res.*, **99**, 2955–2968, 1994.
- Eldholm, O., et al., Summary and preliminary conclusions, ODP Leg 104, *Proc. Ocean Drill. Program, Initial Rep.*, **104**, 751–771, 1987.
- Erlank, A. J., J. S. Marsh, A. R. Duncan, R. M. Miller, C. J. Hawkesworth, P. J. Betton, and D. C. Rex, Geochemistry and petrogenesis of the Etendeka volcanic rocks from SWA/Namibia, *Spec. Publ. Geol. Soc. S. Afr.*, **13**, 195–245, 1984.
- Ewart, A., S. C. Milner, R. A. Armstrong, and A. R. Duncan, Etendeka volcanism of the Goboboseb mountains and

- Messum igneous complex, Namibia. Part 1: geochemical evidence of Early Cretaceous Tristan Plume melts and the role of crustal contamination in the Paraná-Etendeka CBF, *J. Petrol.*, **39**, 191–225, 1998.
- Farnetani, C. G., M. A. Richards, and M. S. Ghiorso, Petrological models of magma evolution and deep crustal structure beneath hotspots and flood basalt provinces, *Earth Planet. Sci. Lett.*, **143**, 81–94, 1996.
- Gallagher, K., and R. Brown, The onshore record of passive margin evolution, *J. Geol. Soc. London*, **154**, 451–457, 1997.
- Gerrard, I., and G. C. Smith, Post Palaeozoic succession and structure of the south-western African continental margin, in *Studies in Continental Margin Geology*, edited by J. Watkins and C. Drake, *AAPG Mem.*, **34**, 49–74, 1982.
- Gladzenko, T. P., K. Hinz, O. Eldholm, H. Meyer, S. Neben, and J. Skogseid, South Atlantic volcanic margins, *J. Geol. Soc. London*, **154**, 465–470, 1997.
- Gladzenko, T. P., J. Skogseid, and O. Eldholm, Namibia volcanic margin, *Mar. Geophys. Res.*, **20**, 313–341, 1998.
- Green, R. W. E., Seismic refraction observations in the Damara Orogen and flanking craton and their bearing on deep seated processes in the orogen, in *The Pan-African Damara Orogen of South West Africa/Namibia*, edited by R. M. Miller, *Spec. Publ. Geol. Soc. S. Afr.*, **11**, 355–367, 1983.
- Haack, U., Reconstruction of the cooling history of the Damara Orogen by correlation of radiometric ages with geography and altitude, in *Intracontinental Fold Belts*, edited by H. Martin and F. Eder, pp. 873–884, Springer-Verlag, New York, 1983.
- Harland, W. B., R. L. Armstrong, A. V. Cox, L. E. Craig, A. G. Smith, and D. G. Smith, *A Geologic Time Scale*, Cambridge Univ. Press, New York, 1990.
- Harris, C., Oxygen isotope geochemistry of the Mesozoic anorogenic complexes of Damaraland, northwest Namibia: Evidence for crustal contamination and its effect on silica saturation, *Contrib. Mineral. Petrol.*, **122**, 308–321, 1995.
- Harris, C., J. S. Marsh, and S. C. Milner, Petrology of the alkaline core of the Messum igneous complex, Namibia: Evidence for the progressively decreasing effect of crustal contamination, *J. Petrol.*, **40**, 1377–1397, 1999.
- Hinz, K., S. Neben, B. Schreckenberger, H. A. Roeser, M. Block, K. Goncalves de Souza, and H. Meyer, The Argentine Continental Margin north of 48°S: Sedimentary successions, volcanic activity during breakup, *Mar. Pet. Geol.*, **16**, 1–25, 1999.
- Holbrook, W. S., G. M. Purdy, R. E. Sheridan, L. Glover III, M. Talwani, J. Ewing, and D. Hutchinson, Seismic structure of the U.S. Mid-Atlantic continental margin, *J. Geophys. Res.*, **99**, 17,871–17,891, 1994a.
- Holbrook, W. S., E. C. Reiter, G. M. Purdy, D. Sawyer, P. L. Stoffa, J. A. Austin Jr., J. Oh, and J. Makris, Deep structure of the U.S. Atlantic continental margin, offshore South Carolina, from coincident ocean bottom and multichannel seismic data, *J. Geophys. Res.*, **99**, 9155–9178, 1994b.
- Holliger, K., and A. Levander, Lower crustal reflectivity modeled by rheological controls on mafic intrusions, *Geology*, **22**, 367–370, 1994.
- IAGA Division V, Working Group 8, International geomagnetic reference field, 1995 revision, *Geophys. J. Int.*, **125**, 318–321, 1996.
- Korn, H., and H. Martin, The Messum igneous complex in south west Africa, *Trans. Geol. Soc. S. Afr.*, **57**, 83–124, 1954.
- Larsen, H. C., et al., Summary and principal results, *Proc. Ocean Drill. Program, Initial Rep.*, **152**, 279–292, 1994.
- Larson, R. L., and J. W. Ladd, Evidence for the opening of the South Atlantic in the Early Cretaceous, *Nature*, **246**, 209–212, 1973.
- Light, M. P. R., M. P. Maslanyi, and N. L. Banks, New geophysical evidence for extensional tectonics on the divergent margin offshore Namibia, in *Magmatism and the Causes of Continental Break-up*, edited by B. C. Storey, T. Alabaster, and R. J. Pankhurst, *Geol. Soc. Spec. Publ.*, **68**, 257–270, 1992.
- Light, M. P. R., M. P. Maslanyi, R. J. Greenwood, and N. L. Banks, Seismic sequence stratigraphy and tectonics offshore Namibia, in *Tectonics and Seismic Sequence Stratigraphy*, edited by G. Williams and A. Dobb, *Geol. Soc. Spec. Publ.*, **71**, 163–191, 1993.
- Ludwig, W. J., J. E. Nafe, and C. L. Drake, Seismic refraction, in *The Sea, vol. 4, part 1*, edited by A. E. Maxwell, pp. 53–84, Wiley-Interscience, New York, 1970.
- Martin, H., M. Mathias, and E. S. W. Simpson, The Damaraland sub-volcanic ring complexes in south west Africa, *Rep. Int. Geol. Congr. XXI Sess.*, **13**, 156–174, 1960.
- Meissner, R., and L. Brown, Seismic reflections from the Earth's crust: Comparative studies of tectonic patterns, *Geophys. J. Int.*, **105**, 1–2, 1991.
- Miller, R. M., *The Pan-African Damara Orogen of South West Africa/Namibia*, *Spec. Publ. Geol. Soc. S. Afr.*, **11**, 1983.
- Milner, S. C., *Geological map of Namibia, sheet 2114, Omaruru, scale 1:250000*, Minist. of Mines and Energy, Geol. Surv. of Namibia and Geol. Surv. of Finl., Windhoek, Namibia, 1997.
- Milner, S. C., and A. P. LeReox, Isotope characteristics of the Okenyanya igneous complex, northwestern Namibia: Constraints on the composition of the early Tristan Plume and the origin of the EM1 mantle component, *Earth Planet. Sci. Lett.*, **141**, 277–291, 1996.
- Milner, S. C., A. P. LeReox, and M. O'Connor, Age of Mesozoic igneous rocks in northwestern Namibia, and their relationship to continental breakup, *J. Geol. Soc. London*, **152**, 97–104, 1995.
- Nürnberg, D., and R. Müller, The tectonic evolution of the South Atlantic from Late Jurassic to present, *Tectonophysics*, **191**, 27–53, 1991.
- O'Connor, J. M., and R. A. Duncan, Evolution of the Walvis Ridge-Rio Grande Rise hot spot system: Implications for African and South American plate motions over plumes, *J. Geophys. Res.*, **95**, 17,475–17,502, 1990.
- Peate, D. W., The Paraná-Etendeka Province, in *Large Igneous Provinces, Geophys. Monogr. Ser.*, vol. 100, edited by J. Mahoney and M. Coffin, pp. 217–246, 1997.
- Planke, S., E. Alvestad, and O. Eldholm, Seismic characteristics of basaltic extrusive and intrusive rocks, *Leading Edge*, **18**, 342–348, 1999.
- Podvin, P., and I. Lecomte, Finite difference computation of traveltimes in very contrasted velocity models: A massively parallel approach and its associated tools, *Geophys. J. Int.*, **105**, 271–284, 1991.
- Porada, H., The Damara-Ribeira orogen of the Pan-African-Braziliano cycle in Namibia (southwest Africa) and Brazil as interpreted in terms of continental collision, *Tectonophysics*, **57**, 237–265, 1979.
- Porada, H., Pan-African rifting and orogenesis in southern equatorial Africa and eastern Brazil, *Precambrian Res.*, **44**, 103–136, 1989.
- Rabinowitz, P. D., and J. LaBrecque, The Mesozoic South Atlantic Ocean and Evolution of Its Continental Margins, *J. Geophys. Res.*, **84**, 5973–6002, 1979.
- Renne, P. R., J. M. Glen, S. C. Milner, and A. R. Duncan, Age of Etendeka flood volcanism and associated intrusions in southwestern Africa, *Geology*, **24**, 659–662, 1996.
- Renne, P. R., M. Ernesto, and S. C. Milner, Geochronology

- of the Paraná-Etendeka magmatic province, *Eos Trans. AGU*, 78(46), Fall Meet. Suppl., F742, 1997.
- Roberts, D. G., et al., Site 555, *Initial Rep. Deep Sea Drill. Proj.*, 81, 277–399, 1984.
- Sandwell, D. T., and W. H. F. Smith, Marine gravity anomaly from Geosat and ERS-1 satellite altimetry, *J. Geophys. Res.*, 102, 10,039–10,054, 1997.
- Saunders, A. D., J. G. Fitton, A. C. Kerr, M. J. Norr, and R. W. Kent, The North Atlantic Igneous Province, in *Large Igneous Provinces*, *Geophys. Monogr. Ser.*, vol. 100, edited by J. Mahoney and M. Coffin, pp. 45–94, 1997.
- Schmitt, A. K., R. Emmermann, B. Buehn, F. Hentjes-Kunst, and R. B. Trumbull,  $^{40}\text{Ar}/^{39}\text{Ar}$  geochronology and petrogenesis of metaluminous and peralkaline granites from the Brandberg complex, Namibia: Evidence for a major mantle contribution, *J. Petrol.*, in press, 2000.
- Schön, J. H., *Physical Properties of Rocks: Fundamentals and Principles of Petrophysics*, vol. 18, Handbook of Geophysical Exploration. Seismic Exploration, 1996.
- Schönharting, G., and N. Abrahamsen, Paleomagnetism of the volcanic sequences in Hole 642E, ODP Leg 104, Vøring Plateau, and correlation with early Tertiary basalts in the North Atlantic, *Proc. Ocean Drill. Program, Sci. Results*, 104, 911–920, 1989.
- Schreckenberger, B., Magnetische Anomalien über seewärts einfallenden seismischen Reflektorfolgen - eine vergleichende Untersuchung verschiedener Vorkommen im Atlantik, Ph.D. thesis, Univ. of Frankfurt, Frankfurt a.M., Germany, 1997.
- Sibuet, J.-C., W. W. Hay, A. Prunier, A. Montadert, K. Hinz, and J. Fritsch, The eastern Walvis Ridge and adjacent basins (South Atlantic): Morphology, stratigraphy, and structural evolution in light of the results of Legs 40 and 75, *Initial Rep. Deep Sea Drill. Proj.*, 75, 483–508, 1984.
- Sleep, N. H., and K. Fuyita, *Principles of Geophysics*, Blackwell Sci., Malden, Mass., 1997.
- Sobolev, S. V., N. Laube, K. Bauer, A. Schulze, and R. Trumbull, Signature of a mantle plume in the seismic velocity structure of the Namibian continental margin, paper presented at *IAVCEI International Volcanological Congress, Cape Town, South Africa, July 11–16*, 1998.
- Talwani, M., J. L. Worzel, and M. Landisman, Rapid gravity computations for two-dimensional bodies with application to the Mendocino submarine fracture zone, *J. Geophys. Res.*, 64, 49–59, 1959.
- Tankard, A. J., M. P. A. Eriksson, D. K. Hobday, D. R. Hunter, and E. E. L. Minter, *Crustal Evolution of Southern Africa: 3.8 Billion Years of Earth History*, Springer-Verlag, New York, 1982.
- Trumbull, R. B., H. Gerstenberger, A. Schmitt, B. Mingram, B. Buehn, and R. Emmermann, Mesozoic igneous complexes in Namibia: Crust-mantle interaction on a rifted continental margin, *Terra Nova*, 9, 459, 1997.
- Turner, S., C. Hawkesworth, K. Gallagher, K. Stewart, D. Peate, and M. Mantovani, Mantle plumes, flood basalts, and thermal models for melt generation beneath continents: Assessment of a conductive heating model and application to the Paraná, *J. Geophys. Res.*, 101, 11,503–11,518, 1996.
- Van der Voo, R., *Paleomagnetism of the Atlantic, Tethys and Iapetus Oceans*, Cambridge Univ. Press, New York, 1993.
- Watts, A. B., and J. D. Fairhead, A process-oriented approach to modeling the gravity signature of continental margins, *Leading Edge*, 17, 258–263, 1999.
- Wessel, P., and W. H. F. Smith, Free software helps map and display data, *Eos Trans. AGU*, 72, 441,445–446, 1991.
- White, R. S., and D. P. McKenzie, Magmatism at rift zones: The generation of volcanic margins and flood basalts, *J. Geophys. Res.*, 94, 7685–7729, 1989.
- White, R. S., G. D. Spence, S. R. Fowler, D. P. McKenzie, G. K. Westbrook, and A. N. Bowen, Magmatism at rifted continental margins, *Nature*, 330, 439–444, 1987.
- Zelt, C. A., Modelling strategies and model assessment for wide-angle seismic traveltimes, *Geophys. J. Int.*, 139, 183–204, 1999.
- Zelt, C. A., and R. M. Ellis, Practical and efficient ray-tracing in two-dimensional media for rapid traveltimes and amplitudes forward modelling, *Can. J. Explor. Geophys.*, 24, 16–31, 1988.
- Zelt, C. A., and R. B. Smith, Seismic traveltimes inversion for 2-D crustal velocity structure, *Geophys. J. Int.*, 108, 16–34, 1992.
- 
- K. Bauer, R. Emmermann, A. Schulze, and R.B. Trumbull, GeoForschungsZentrum Potsdam (GFZ), Telegrafenberg, D-14473 Potsdam, Germany. (klaus@gfz-potsdam.de; emmermann@gfz-potsdam.de; robert@gfz-potsdam.de; bobby@gfz-potsdam.de)
- N. Fechner and K. Gohl, Alfred-Wegener-Institut für Polar- und Meeresforschung, Columbusstrasse, D-27568 Bremerhaven, Germany. (kgohl@awi-bremerhaven.de)
- K. Hinz, S. Neben, and B. Schreckenberger, Bundesanstalt für Geowissenschaften und Rohstoffe, POB 510153, D-3000 Hannover 51, Germany. (k.hinz@bgr.de; s.neben@bgr.de; b.schreckenberger@bgr.de)
- K. Weber, Institut für Geologie und Dynamik der Lithosphäre, Goldschmidstr. 3, D-33077 Göttingen, Germany. (kweber@gwdg.de)

(Received September 17, 1999; revised May 23, 2000; accepted June 14, 2000.)